Journal of Computational Physics 492 (2023) 112429

Contents lists available at ScienceDirect

Journal of Computational Physics

journal homepage: www.elsevier.com/locate/jcp

On high order positivity-preserving well-balanced finite volume methods for the Euler equations with gravitation

Yupeng Ren [a], Kailiang Wu [b,1], Jianxian Qiu [c,2], Yulong Xing [d,*,3]

[a] Beijing Computational Science Research Center, Beijing 100193, PR China
[b] Department of Mathematics & SUSTech International Center for Mathematics, Southern University of Science and Technology, and National Center for Applied Mathematics Shenzhen (NCAMS), Shenzhen, Guangdong 518055, PR China
[c] School of Mathematical Sciences and Fujian Provincial Key Laboratory of Mathematical Modeling and High-Performance Scientific Computing, Xiamen University, Xiamen, Fujian 361005, PR China
[d] Department of Mathematics, The Ohio State University, Columbus, OH 43210, USA

ARTICLE INFO

Article history:
Received 14 December 2022
Received in revised form 14 June 2023
Accepted 11 August 2023
Available online 21 August 2023

Keywords:
Compressible Euler equations
Gravitational field
Weighted essentially non-oscillatory methods
Positivity preserving
Well-balanced

ABSTRACT

This paper studies three high-order structure-preserving finite volume weighted essentially non-oscillatory (WENO) methods, which are not only well balanced (WB) for a general known hydrostatic equilibrium state but also preserve the positivity of density and pressure, for the compressible Euler equations under gravitational fields. These methods are built on a simple local scaling positivity-preserving (PP) limiter and a modified WENO-ZQ reconstruction exactly preserving the cell average value and scaling invariance. The WB properties of these three methods are achieved based on suitable numerical fluxes and approximation to the gravitational source terms. Based on some convex decomposition techniques as well as several critical properties of the admissible states and numerical flux, we carry out rigorous positivity-preserving analyses for these three WB schemes. We rigorously prove that the three WB methods, coupled with the PP limiter and a strong-stability-preserving time discretization, are always PP under suitable Courant-Friedrichs-Lewy conditions. Extensive numerical examples are provided to confirm WB and PP properties of three methods.

1. Introduction

Euler equations with gravitational source terms play an important role in many application fields, such as astrophysics and atmospheric science. This model can be formulated as

$$\mathbf{U}_t + \nabla \cdot \mathbf{F}(\mathbf{U}) = \mathbf{S}(\mathbf{U}, \mathbf{x}) \tag{1.1}$$

with

* Corresponding author.
E-mail addresses: ypren@stu.xmu.edu.cn (Y. Ren), wukl@sustech.edu.cn (K. Wu), jxqiu@xmu.edu.cn (J. Qiu), xing.205@osu.edu (Y. Xing).

[1] The work of this author is partially supported by National Natural Science Foundation of China grant 12171227 and Shenzhen Science and Technology Program grant RCJC20221008092757098.
[2] The work of this author is partially supported by National Key Research and Development Program of China grant 2022YFA1004501 and National Natural Science Foundation of China grant 12071392.
[3] The work of this author is partially supported by National Science Foundation grants DMS-1753581 and DMS-2309590.

https://doi.org/10.1016/j.jcp.2023.112429
0021-9991/

$$\mathbf{U}=\begin{pmatrix}\rho\\ \mathbf{m}\\ E\end{pmatrix},\quad \mathbf{F}(\mathbf{U})=\begin{pmatrix}\rho\mathbf{u}\\ \rho\mathbf{u}\otimes\mathbf{u}+p\mathbf{I}_d\\ (E+p)\mathbf{u}\end{pmatrix},\quad \mathbf{S}(\mathbf{U},\mathbf{x})=\begin{pmatrix}0\\ -\rho\nabla\phi\\ -\mathbf{m}\cdot\nabla\phi\end{pmatrix}, \tag{1.2}$$

where $\mathbf{x}\in\Omega\subseteq\mathbb{R}^d$; ρ, $\mathbf{m}$ and E denote the density, momentum vector, and total energy, respectively; $\mathbf{I}_d$ is the identity matrix of size d; $\mathbf{u}=\mathbf{m}/\rho$ is velocity. The source term $\mathbf{S}(\mathbf{U},\mathbf{x})$ represents the effect of the static gravitational field, and the $\phi(\mathbf{x})$ is the gravitational potential. The total energy $E=\rho e+\frac{\|\mathbf{m}\|^2}{2\rho}$ with e being the specific internal energy, which is related to pressure p and density ρ through an equation of state (EoS). A general EoS can be expressed as $e=\mathscr{E}(\rho,p)$. For ideal gases, it is given by

$$p=(\gamma-1)\rho e=(\gamma-1)\left(E-\frac{\|\mathbf{m}\|^2}{2\rho}\right), \tag{1.3}$$

where the constant $\gamma\in(1,+\infty)$ is the adiabatic index.

System (1.1)-(1.2) with an EoS forms a hyperbolic system which is typically called a balance law. Such a system admits non-trivial hydrostatic equilibrium solutions, in which the gravitational source term and flux gradient are balanced exactly at the discrete level, and perturbations of such hydrostatic equilibrium solutions often appear in atmospheric and astrophysical applications. However, using standard numerical methods to solve (1.1)-(1.2) may not be able to preserve the balance, and can result in large numerical errors when simulating equilibrium solutions and their perturbations, unless the simulation is carried out on much refined meshes, which can be time-consuming for multi-dimensional problems. In order to address the issue, researchers propose well-balanced (WB) methods that preserve precisely the discrete versions of hydrostatic equilibrium solutions up to machine accuracy, so as to effectively capture the equilibria and their perturbations on relatively coarse meshes. The exploration of WB numerical schemes originally arose from solving the shallow water equations on a non-flat bottom topology, which is another hyperbolic balance laws model; see, for example, [1,14,39,43,44]. In recent years, researchers have witnessed growing interest in developing WB schemes for Euler equations (1.1)-(1.2) with gravitation, and many efforts have been done in this direction, including the finite volume (FV) WB methods [4,6,15,18–20,22,23], the gas-kinetic schemes [27,45], finite difference methods [11,26,41], and discontinuous Galerkin (DG) methods [7,24,25,31,37,52]. Most of these methods require that the equilibrium solutions are known a priori. Recently, some efforts have been made to design WB methods without a prior knowledge of hydrostatic equilibrium solutions; see, e.g., [3,9,10,19,30].

In physics, the density and pressure are positive. It is required that numerical schemes maintain their positivity at the discrete level, which is necessary not only for the physical significance of numerical solutions but also for the robustness of numerical schemes. However, most high-order schemes for the system (1.1)-(1.2) usually do not have the positivity-preserving (PP) property, and therefore there is a risk of failure in simulating problems with low density, low pressure, and/or strong shocks. In the past decade, high-order PP, or more generally bound-preserving, numerical schemes have been developed for a wide variety of hyperbolic systems. There are two main approaches mostly studied in the literature. One is based on the limiter for the reconstruction of polynomials, cf. [33,35,43,47,49,50]. The other one is based on flux correction limiters [16,38,46]. We refer to [28] for more discussion on bound-preserving schemes. Based on the first approach, high-order PP DG schemes were designed for the Euler equations without source term in [50] and with various source terms including the gravitational source term in [51]. The bound-preserving numerical methods were also developed for, for example, the shallow water equations [40,43], the special relativistic Euler equations [34,38], the compressible Navier–Stokes equations [47], and the ideal magnetohydrodynamic equations [33,35], and the general relativistic Euler equations under strong gravitational fields [32], to name a few. Recently, a geometric quasilinearization framework was proposed in [36] for studying bound-preserving problems involving nonlinear constraints, with applications to various physical systems including Euler equations. We would like to mention that, for the shallow water equations, several high-order PP WB schemes have been proposed, for example, in [21,42,43]. Very recently, uniformly high-order PP WB methods were proposed in the DG framework [37,52] and the central DG framework [17] for the Euler equations with gravitation.

The first goal of this paper is to propose a high-order FV weighted essentially non-oscillatory (WENO) scheme (abbreviated as "`New-WB`" scheme for convenience), which has both WB and PP properties. While most existing methods have only one of these two attributes, our `New-WB` scheme achieves both properties by generalizing the recently developed PP WB DG scheme [37] into the FV framework. In the `New-WB` scheme, the WB discretization of the source term is motivated by [23], by reformulating the gravitational source term in the momentum equations based on the cell average value of the numerical solution and the assumption that the equilibrium solutions are known a priori. In the FV framework used in this study, only the average values of the equilibrium solutions are required a priori. In order to accommodate the PP property in theory, we also discretize the source term in the energy equation in the same fashion as in the momentum equations, while such a careful treatment was not considered in [23] for the consideration of WB property only. A modified version of the WENO-ZQ [53] reconstruction was adopted in the `New-WB` scheme to preserve the scaling-invariant property, which is advantageous to avoid oscillation near the shock wave for multi-scale problems. Another significant difference from [23] is the choice of numerical fluxes. Different from the modified Lax-Friedrichs (LF) flux in [23,24], we adopt an appropriately modified HLLC numerical flux. There are two reasons for such a choice. First, the HLLC flux can be modified in a unified way to achieve the WB property for different types of hydrostatic equilibrium solutions, while the WB modification of the LF flux relies heavily on specific problems. Secondly, the modified HLLC flux retains the desired PP property, while the PP

property of the modified LF flux [23,24] is questionable in such a framework. The present New-WB FV scheme overcomes some shortcomings in the PP WB DG schemes [37], which need an extra slope limiter to suppress spurious oscillations when simulating problems with strong discontinuities.

Another goal of this paper is to rigorously analyze and enforce the PP property for the two existing high-order WB methods developed in the literature. One WB method was proposed by Grosheintz-Laval and Käppeli in [15] (abbreviated as "GLK-WB" scheme), which is based on a new local hydrostatic reconstruction. This scheme satisfies the WB property for any consistent numerical fluxes. The other WB method was developed by Klingenberg, Puppo, Semplice in [20] (abbreviated as "KPS-WB" scheme), which assumes that the desired hydrostatic equilibrium solutions are known. The KPS-WB scheme is based on a high-order reconstruction of fluctuation from equilibrium density, velocity, and pressure balance, and is based on a WB quadrature of the source term. In addition to consistency, the numerical flux in this scheme does not require any modifications.

We reformulate these two numerical methods in an equivalent form, so that the framework to prove the PP property of the New-WB FV scheme method can be adopted. Our analyses show that the New-WB and GLK-WB schemes have similar conclusions on the PP property, while that of the KPS-WB scheme is slightly different due to the use of Romberg's method in the discretization of the source term. We will also present extensive numerical examples, to validate the WB property of our New-WB method as well as the PP property of the above three methods. The results confirm that under suitable Courant-Friedrichs-Lewy (CFL) conditions, all these three schemes achieve both the WB and PP properties.

The paper is organized as follows. In Section 2, we introduce hydrostatic equilibrium solutions, several properties of the admissible state set, the FV discretization of one-dimensional (1D) and two-dimensional (2D) Euler systems, and a modified WENO-ZQ reconstruction. Our main results on PP properties are outlined in Section 3, which hold for all three methods. In Sections 4-6, we introduce the numerical fluxes and discretizations of source terms involved in each of the three WB methods respectively, and present rigorous analyses of the PP property. Some numerical examples to verify the desired properties and effectiveness of the proposed schemes are given in Section 7, before the concluding remark in Section 8.

2. Preliminaries

In this section, we first introduce stationary hydrostatic equilibrium solutions of system (1.1)-(1.2), and a set of physically admissible states followed by some Lemmas, which will be used in the sections below. Next, we present the discretization of the 1D and 2D Euler systems in the FV framework and introduce a modified WENO-ZQ reconstruction which preserves the scaling-invariant property and will be used in our method.

2.1. Stationary hydrostatic solutions

The Euler system with a gravitational source term (1.1)-(1.2) has non-trivial steady-state solutions, where source terms exactly balance flux terms. The zero-velocity hydrostatic equilibrium solution takes the following form

$$\rho = \rho(\mathbf{x}), \quad \mathbf{u} = \mathbf{0}, \quad \nabla p = -\rho \nabla \phi. \tag{2.1}$$

In most cases, we are interested in particular equilibrium states, with typical cases being isothermal and polytropic [18] equilibrium states under the assumption of ideal gas laws. For an isothermal hydrostatic state with the constant temperature $T(\mathbf{x}) \equiv T_0$, the equilibrium solution takes the form

$$\rho^e = \rho_0 \exp\left(-\frac{\phi}{RT_0}\right), \qquad \mathbf{u} = \mathbf{0}, \qquad p^e = p_0 \exp\left(-\frac{\phi}{RT_0}\right),$$

where R is the gas constant, and p_0, ρ_0 are positive constants satisfying $p_0 = \rho_0 R T_0$. A polytropic equilibrium state satisfying the relation $p = K_0 \rho^\gamma$, is given by

$$\rho^e = \left(\frac{\gamma - 1}{K_0 \gamma}(C - \phi)\right)^{\frac{1}{\gamma - 1}}, \quad \mathbf{u} = \mathbf{0}, \quad p^e = \frac{1}{K_0^{\frac{1}{\gamma-1}}}\left(\frac{\gamma - 1}{\gamma}(C - \phi)\right)^{\frac{\gamma}{\gamma-1}},$$

with constants K_0 and C.

For the general EoS, hydrostatic equilibrium solutions have the following expression

$$\mathbf{U}^e(\mathbf{x}) = \left(\rho^e(\mathbf{x}), \mathbf{0}, \rho^e(\mathbf{x})\mathscr{E}\left(\rho^e(\mathbf{x}), p^e(\mathbf{x})\right)\right)^\top, \tag{2.2}$$

for given equilibrium functions $\rho^e(\mathbf{x})$, $p^e(\mathbf{x})$ satisfying (2.1).

2.2. Properties of admissible states

The density ρ and the pressure p must be positive in physics, which means the conserved variable $\mathbf{U}$ should belong to the set

$$G_0 := \left\{ \mathbf{U} = (\rho, \mathbf{m}, E)^\top : \ \rho > 0, \ p > 0 \right\}. \tag{2.3}$$

Assume the general EoS satisfies

$$\text{if} \quad \rho > 0, \quad \text{then} \quad p > 0 \iff e > 0. \tag{2.4}$$

Then, as studied in [50], $\mathbf{U} \in G_0$ is equivalent to $\mathbf{U} \in G$, where

$$G := \left\{ \mathbf{U} = (\rho, \mathbf{m}, E)^\top : \ \rho > 0, \ \widetilde{E} = \rho e = E - \frac{\|\mathbf{m}\|^2}{2\rho} > 0 \right\} \tag{2.5}$$

is a convex set. Next, we introduce two Lemmas for the set G, which have been discussed in [37].

Lemma 2.1 *([37]). If $\mathbf{U} \in G$, it holds that $\lambda \mathbf{U} \in G$ for any $\lambda \in \mathbb{R}^+$. Furthermore, for any $\mathbf{U}_0 \in \overline{G}$ (the closure of G) and constant $\lambda_0 \geq 0$, we have $\lambda \mathbf{U} + \lambda_0 \mathbf{U}_0 \in G$.*

Lemma 2.2 *([37]). For any constant $\lambda \geq 0$, $\delta \in \mathbb{R}$, $\mathbf{U} \in G$, and $\mathbf{a} \in \mathbb{R}^d$, we have*

$$\lambda \mathbf{U} + \delta \big(0, \rho \mathbf{a}, \mathbf{m} \cdot \mathbf{a}\big)^\top \in \overline{G}, \qquad \text{if} \ \ |\delta| \frac{\|\mathbf{a}\|}{\sqrt{2e}} \leq \lambda.$$

2.3. The finite volume discretization and notations

1D spatial discretization: In the 1D case, the Euler system (1.1)-(1.2) reduces to

$$\mathbf{U}_t + \mathbf{F}(\mathbf{U})_x = \mathbf{S}(\mathbf{U}, x), \tag{2.6}$$

with

$$\mathbf{U} = \begin{pmatrix} \rho \\ m \\ E \end{pmatrix}, \quad \mathbf{F}(\mathbf{U}) = \begin{pmatrix} \rho u \\ \rho u^2 + p \\ (E + p) u \end{pmatrix}, \quad \mathbf{S}(\mathbf{U}, x) = \begin{pmatrix} 0 \\ -\rho \phi_x \\ -m \phi_x \end{pmatrix}. \tag{2.7}$$

Assume that the spatial domain Ω is divided into cells $I_j = [x_{j-\frac{1}{2}}, x_{j+\frac{1}{2}}]$, with mesh size $\Delta x_j = x_{j+\frac{1}{2}} - x_{j-\frac{1}{2}}$. We assume the mesh is uniform for ease of presentation, i.e., $\Delta x_j = \Delta x$. The center of cell I_j is denoted by $x_j = (x_{j-\frac{1}{2}} + x_{j+\frac{1}{2}})/2$. The semidiscrete FV numerical scheme for (2.6) takes the form

$$\frac{\mathrm{d}\overline{\mathbf{U}}_j}{\mathrm{d}t} = \mathbf{L}_j(\overline{\mathbf{U}}) := -\frac{1}{\Delta x} \left(\widehat{\mathbf{F}}_{j+\frac{1}{2}} - \widehat{\mathbf{F}}_{j-\frac{1}{2}} \right) + \overline{\mathbf{S}}_j, \tag{2.8}$$

where $\overline{\mathbf{U}}_j = \overline{\mathbf{U}}_j(t)$ is the computational variable to approximate the cell average of the exact solution, $\overline{\mathbf{U}}(x_j, t) = \frac{1}{\Delta x} \int_{I_j} \mathbf{U}(x, t) \mathrm{d}x$. The term $\widehat{\mathbf{F}}_{j\pm\frac{1}{2}} = \mathscr{F}(\mathbf{U}^-_{j\pm\frac{1}{2}}, \mathbf{U}^+_{j\pm\frac{1}{2}})$ is a suitable numerical flux, in which $\mathbf{U}^\pm_{j+\frac{1}{2}}$ are high-order pointwise approximations to $\mathbf{U}(x_{j+\frac{1}{2}}, t)$ from left and right, respectively. The source term approximation is denoted by $\overline{\mathbf{S}}_j = \big(0, \overline{S}^{[2]}_j, \overline{S}^{[3]}_j\big)^\top$ with $\overline{S}^{[\ell]}_j \approx \frac{1}{\Delta x} \int_{I_j} S^{[\ell]} \mathrm{d}x$, in which the ℓ indicates the ℓth element of source term $\mathbf{S}$. The specific numerical fluxes and source term approximation which lead to WB and PP properties will be detailed in the following sections. If the forward Euler time discretization is applied to (2.8), we have

$$\overline{\mathbf{U}}^{n+1}_j = \overline{\mathbf{U}}^n_j + \Delta t \mathbf{L}_j(\mathbf{U}^n) = \overline{\mathbf{U}}^n_j - \frac{\Delta t}{\Delta x} \left(\widehat{\mathbf{F}}_{j+\frac{1}{2}} - \widehat{\mathbf{F}}_{j-\frac{1}{2}} \right) + \Delta t \overline{\mathbf{S}}^n_j, \tag{2.9}$$

where Δt is the time step size and the superscript n represents the nth time level.

Multi-dimensional spatial discretization: For ease of presentation, we only discuss it for 2D Euler equations with gravity field, which are given by

$$\mathbf{U}_t + \mathbf{F}(\mathbf{U})_x + \mathbf{G}(\mathbf{U})_y = \mathbf{S}(\mathbf{U}, x, y), \tag{2.10}$$

with

$$\mathbf{U}=\begin{pmatrix}\rho\\ m\\ n\\ E\end{pmatrix},\ \mathbf{F}=\begin{pmatrix}\rho u\\ \rho u^2+p\\ \rho uv\\ (E+p)u\end{pmatrix},\ \mathbf{G}=\begin{pmatrix}\rho v\\ \rho uv\\ \rho v^2+p\\ (E+p)v\end{pmatrix},\ \textit{and}\ \mathbf{S}=\begin{pmatrix}0\\ -\rho\phi_x\\ -\rho\phi_y\\ -\rho u\phi_x-\rho v\phi_y\end{pmatrix}. \tag{2.11}$$

Here $\mathbf{u}=(u,v)$ and $\mathbf{m}=(\rho u,\rho v)$, with u and v being the velocity in $x-$ and $y-$ directions, respectively, and

$$m=\rho u,\quad n=\rho v,\quad E=\frac{1}{2}\rho(u^2+v^2)+\rho e.$$

Assume that the computational domain is discretized into rectangular meshes $I_{ij}=\{[x_{i-\frac{1}{2}},x_{i+\frac{1}{2}}]\times[y_{j-\frac{1}{2}},y_{j+\frac{1}{2}}]\}$, with mesh sizes $\Delta x_i=x_{i+\frac{1}{2}}-x_{i-\frac{1}{2}}$ and $\Delta y_j=y_{j+\frac{1}{2}}-y_{j-\frac{1}{2}}$ in x- and y-directions, respectively. For simplicity, uniform meshes are assumed, that is $\Delta x_i=\Delta x$ and $\Delta y_j=\Delta y$. The semidiscrete FV numerical scheme is given by

$$\frac{d\overline{\mathbf{U}}_{ij}}{dt}=\mathbf{L}_{ij}(\overline{\mathbf{U}}):=-\frac{1}{\Delta x}(\widehat{\mathbf{F}}_{i+\frac{1}{2},j}-\widehat{\mathbf{F}}_{i-\frac{1}{2},j})-\frac{1}{\Delta y}(\widehat{\mathbf{G}}_{i,j+\frac{1}{2}}-\widehat{\mathbf{G}}_{i,j-\frac{1}{2}})+\overline{\mathbf{S}}_{ij}, \tag{2.12}$$

where $\overline{\mathbf{U}}_{ij}=\overline{\mathbf{U}}_{ij}(t)$ is the 2D computational variable which approximates $\frac{1}{|I_{ij}|}\int_{I_{ij}}\mathbf{U}(\mathbf{x},t)\mathrm{d}\mathbf{x}$ with $|I_{ij}|=\Delta x_i\Delta y_j$. Here, $\widehat{\mathbf{F}}_{i+\frac{1}{2},j}$ is the numerical flux at the x-direction, which is an approximation to $\frac{1}{\Delta y}\int_{y_{j-\frac{1}{2}}}^{y_{j+\frac{1}{2}}}\mathbf{F}(\mathbf{U}(x_{j+\frac{1}{2}},y))\mathrm{d}y$. Similarly, $\widehat{\mathbf{G}}_{i,j+\frac{1}{2}}$ is the numerical flux at the y-direction. The source term approximation is denoted by $\overline{\mathbf{S}}_{ij}$. The specific numerical fluxes and source term approximation which lead to WB and PP properties will be detailed in the following sections. Combining the semidiscrete FV scheme (2.12) with the forward Euler time discretization leads to

$$\overline{\mathbf{U}}_{ij}^{n+1}=\overline{\mathbf{U}}_{ij}^{n}-\lambda_1(\widehat{\mathbf{F}}_{i+\frac{1}{2},j}-\widehat{\mathbf{F}}_{i-\frac{1}{2},j})-\lambda_2(\widehat{\mathbf{G}}_{i,j+\frac{1}{2}}-\widehat{\mathbf{G}}_{i,j-\frac{1}{2}})+\Delta t\overline{\mathbf{S}}_{ij}^{n}, \tag{2.13}$$

where $\lambda_1=\Delta t/\Delta x$, $\lambda_2=\Delta t/\Delta y$.

SSP-RK time discretization: In general, explicit strong-stability-preserving (SSP) Runge-Kutta (RK) methods [13] are used as the high-order temporal discretization. In this paper, the third-order accurate SSP RK method is used, which takes the form

$$\begin{aligned}\mathbf{U}^{(1)}&=\overline{\mathbf{U}}^{n}+\Delta t\mathbf{L}(\overline{\mathbf{U}}^{n}),\\ \mathbf{U}^{(2)}&=\frac{3}{4}\overline{\mathbf{U}}^{n}+\frac{1}{4}\Big(\mathbf{U}^{(1)}+\Delta t\mathbf{L}(\mathbf{U}^{(1)})\Big),\\ \overline{\mathbf{U}}^{n+1}&=\frac{1}{3}\overline{\mathbf{U}}^{n}+\frac{2}{3}\Big(\mathbf{U}^{(2)}+\Delta t\mathbf{L}(\mathbf{U}^{(2)})\Big).\end{aligned} \tag{2.14}$$

2.4. WENO-ZQ reconstruction

The cell interface values $\mathbf{U}^{\pm}_{j+\frac{1}{2}}$ are obtained from the cell averages $\overline{\mathbf{U}}_j$ via a reconstruction procedure. In this paper, we will use a modified version of the WENO-ZQ reconstruction developed by Zhu and Qiu in [53]. A similar modification was also studied in [8] for the motivation of ensuring the scaling-invariant property. The WENO-ZQ reconstruction, instead of the traditional WENO reconstruction, was chosen in this paper, due to the fact that it satisfies the average-value-preserving property, and we refer to Section 3.1 for the detailed discussion on this. The 1D fifth-order modified WENO-ZQ reconstruction procedure is presented below as an example, and the multi-dimensional extension can be obtained in a similar fashion through the dimension-by-dimension approach.

From the average value sequence $\{\overline{U}_l\}_{l=j-2}^{j+2}$, we can reconstruct cell interface values $U^{+}_{j-\frac{1}{2}}$, $U^{-}_{j+\frac{1}{2}}$, and Gauss-Lobatto point values $U(x_j^v)$ in the cell I_j in the following way:

- **Step 1**: Take a big stencil $\mathbb{T}_1=\{I_{j-2},\cdots,I_{j+2}\}$, and two small stencils $\mathbb{T}_2=\{I_{j-1},I_j\}$, $\mathbb{T}_3=\{I_j,I_{j+1}\}$, we compose a quartic polynomial $p_1(x)$ and two linear polynomials $p_2(x)$ and $p_3(x)$ satisfying (see Fig. 2.1)

$$\frac{1}{\Delta x}\int_{I_l}p_1(x)dx=\overline{U}_l,\qquad l=j-2,\cdots,j+2, \tag{2.15}$$

$$\frac{1}{\Delta x}\int_{I_l}p_2(x)dx=\overline{U}_l,\ l=j-1,j;\qquad \frac{1}{\Delta x}\int_{I_l}p_3(x)dx=\overline{U}_l,\ l=j,j+1. \tag{2.16}$$

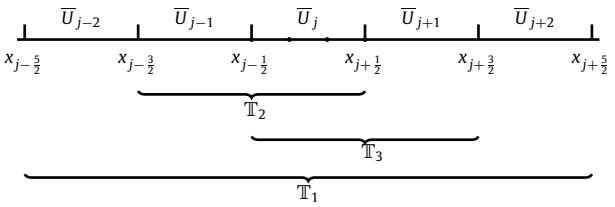

Fig. 2.1. Stencils of WENO-ZQ reconstruction to reconstruct the values at solid circles.

- **Step 2**. In the nonlinear WENO reconstructions, $U(x_j^\nu)$ are computed as a convex combination of these three corresponding polynomial values

$$U(x_j^\nu) = \widetilde{\omega}_1 \left(\frac{1}{\gamma_1} p_1(x_j^\nu) - \frac{\gamma_2}{\gamma_1} p_2(x_j^\nu) - \frac{\gamma_3}{\gamma_1} p_3(x_j^\nu) \right) + \widetilde{\omega}_2 p_2(x_j^\nu) + \widetilde{\omega}_3 p_3(x_j^\nu),$$

where the parameters γ_n $(n = 1, 2, 3)$ and $\widetilde{\omega}_n$ $(n = 1, 2, 3)$ are named linear and nonlinear weights. The weights $\{\gamma_n\}$ can be any positive constants satisfying $\gamma_1 + \gamma_2 + \gamma_3 = 1$ and $\{\widetilde{\omega}_n\}$ are computed from

$$\widetilde{\omega}_n = \frac{\overline{\omega}_n}{\sum_{l=1}^3 \overline{\omega}_l}, \qquad \overline{\omega}_n = \gamma_n \left(1 + \left(\frac{\tau_0}{\varepsilon + \beta_n} \right)^4 \right), \qquad n = 1, 2, 3, \tag{2.17}$$

in which $\varepsilon = \Delta x^2 \max_{l \in \mathbb{T}_1} |\overline{U}_l| + 10^{-12}$, where 10^{-12} is added to avoid zero denominator, and

$$\tau_0 = \frac{|\beta_1 - \beta_2| + |\beta_1 - \beta_3|}{2}, \quad \beta_n = \sum_{\alpha=1}^{r} \int_{I_j} \Delta x^{2\alpha-1} \left(\frac{d^\alpha p_n(x)}{dx^\alpha} \right)^2 dx, \quad n = 1, 2, 3,$$

where $r = 4$ for $n = 1$, and $r = 1$ for $n = 2, 3$.

In fact, we have constructed a polynomial $U(x)$ on the cell I_j in the WENO-ZQ reconstruction, that is

$$U(x) = \frac{\widetilde{\omega}_1}{\gamma_1} p_1(x) + \left(\widetilde{\omega}_2 - \frac{\widetilde{\omega}_1 \gamma_2}{\gamma_1} \right) p_2(x) + \left(\widetilde{\omega}_3 - \frac{\widetilde{\omega}_1 \gamma_3}{\gamma_1} \right) p_3(x), \tag{2.18}$$

and can use this polynomial to evaluate the cell interface values and Gauss-Lobatto point values.

Remark 2.1. It is worth noting that our choice of nonlinear weights (2.17) are slightly different from those in the traditional WENO-ZQ scheme [53], which may lead to large oscillation or overfit phenomenon near the shock wave for some multi-scale problems. Such a modification is advantageous (see the comparison in Fig. 7.1), and it was also used in [8] to ensure the scaling-invariant property.

For the WENO-ZQ reconstruction in the 2D case, we consider rectangular meshes in this paper. The standard dimension-by-dimension approach is given as follows. Starting from cell averages of the function U in both x and y directions, we first perform a 1D WENO-ZQ reconstruction in one direction (e.g. y-direction) to obtain the 1D cell average of the function U in the other direction (e.g. x-direction). Then we apply the WENO-ZQ reconstruction in the other direction to compute the approximate point values. More details can be found in [53].

3. Main results

In this section, we first introduce some unified notations to be used in the description of these three methods. The main results on the PP property are summarized here, and the detailed proof for each method will be presented in the following sections.

3.1. Notations

First of all, two sets of numerical quadrature rules will be used in this paper, namely, the Gauss-Lobatto quadrature for `New-WB` and `GLK-WB` methods, and Romberg's numerical quadrature for `KPS-WB` method. Let k be the algebraic precision of two numerical quadratures.

Table 3.1
Notations to be used in numerical methods.

$\overline{\mathbf{U}}_j = (\overline{\rho}_j, \overline{\mathbf{m}}_j, \overline{E}_j)$	Represents the 1D numerical solution in the cell I_j
$\overline{\mathbf{U}}_{ij} = (\overline{\rho}_{ij}, \overline{\mathbf{m}}_{ij}, \overline{E}_{ij})$	Represents the 2D numerical solution in the cell I_{ij}
$\mathbf{U}(\mathbf{x}) = (\rho(\mathbf{x}), \mathbf{m}(\mathbf{x}), E(\mathbf{x}))$	WENO reconstructed polynomial function from cell averages
$\overline{\rho^e}, \overline{p^e}, \overline{e^e}, \overline{\rho e^e}$	Represent the average of the targeting equilibrium variables
$\rho^e(\mathbf{x}), p^e(\mathbf{x}), e^e(\mathbf{x})$	Represent the equilibrium density, pressure and internal energy
$\mathscr{L}_j(\cdot)$	The 1D discrete average operator with L-point Gauss-Lobatto quadrature and algebraic precision k in the cell I_j
$\mathscr{L}_{ij}(\cdot)$	The 2D discrete average operator with L^2-point Gauss-Lobatto quadrature and algebraic precision k in the cell I_{ij}
$\mathscr{R}_j(\cdot), \mathscr{R}_{ij}(\cdot)$	Similar to the definition of $\mathscr{L}_j(\cdot)$, $\mathscr{L}_{ij}(\cdot)$, with Romberg's quadrature used
$\mathscr{W}_j\left(\{\overline{U}_l\}\right)$	The 1D WENO reconstruction operator on the cell I_j
$\mathscr{W}_{ij}\left(\{\overline{U}_{g,l}\}\right)$	The 2D WENO reconstruction operator on the cell I_{ij}
$\tau, \widetilde{\tau}$	The 1D and 2D WB correction term for the source term approximation

- `New-WB` and `GLK-WB` methods
  In the 1D case, let $\mathbb{S}_j = \{x_j^\nu\}_{\nu=1}^L$ be the set of L-point Gauss-Lobatto quadrature nodes on cell I_j, and the quadrature weights are $\{\omega_\nu\}_{\nu=1}^L$ with $\omega_1 = \omega_L = \frac{1}{L(L-1)}$, where $L \geq (k+3)/2$.
  In the 2D case, let $\{x_i^\nu\}_{\nu=1}^L$ and $\{y_j^\nu\}_{\nu=1}^L$ denote L-point ($L \geq (k+3)/2$) Gauss-Lobatto quadrature nodes with weights $\{\omega_\nu\}$ on the cell $[x_{i-\frac{1}{2}}, x_{i+\frac{1}{2}}]$ and $[y_{j-\frac{1}{2}}, y_{j+\frac{1}{2}}]$, respectively. Let the $\mathbb{S}_{ij} = \{\mathbf{x}_{ij}^q\}_{q=1}^{L^2}$ be quadrature nodes in the cell I_{ij}, and quadrature weights are $\{\hat{\omega}_q\} = \{\omega_\nu\} \bigotimes \{\omega_\nu\}$.
- `KPS-WB` method
  In the 1D case, let $\mathbb{S}_j = \{x_j^\kappa\}_{\kappa=1}^N$ and $\{\omega_\kappa\}_{\kappa=1}^N$ be the set of N-point Romberg's quadrature nodes and weights on the cell I_j, where $N \geq 2^{\frac{k-1}{2}} + 1$, and the nodes are given by $x_j^\kappa = x_{j-\frac{1}{2}} + \frac{(\kappa-1)}{N-1}\Delta x$.
  In the 2D case, let $\{x_i^\kappa\}_{\kappa=1}^N$ and $\{y_j^\kappa\}_{\kappa=1}^N$ denote N-point Romberg's quadrature nodes with weight $\{\omega_\kappa\}$ in the intervals $[x_{i-\frac{1}{2}}, x_{i+\frac{1}{2}}]$ and $[y_{j-\frac{1}{2}}, y_{j+\frac{1}{2}}]$, respectively. Let $\mathbb{S}_{ij} = \{\mathbf{x}_{ij}^q\}_{q=1}^{N^2}$ quadrature nodes in the cell I_{ij}, and quadrature weights are $\{\hat{\omega}_q\} = \{\omega_\kappa\} \bigotimes \{\omega_\kappa\}$.

Definition 3.1. We introduce the notations $\mathscr{L}_j(\cdot)$ and $\mathscr{R}_j(\cdot)$ to be the 1D discrete average operators, which compute the integral over the cell I_j using the Gauss-Lobatto quadrature and Romberg's quadrature respectively. Similarly, let $\mathscr{L}_{ij}(\cdot)$ and $\mathscr{R}_{ij}(\cdot)$ to be the 2D discrete average operators over the cell I_{ij}.

Definition 3.2. Let the notation $\mathscr{W}_j\left(\{\overline{U}_l\}\right)$ to be the 1D WENO reconstruction operator on the cell I_j, which outputs the reconstructed polynomial $U(x)$ in (2.18) with $(k+1)$th order accuracy from the cell averages $\{\overline{U}_l\}$. Similarly, let $\mathscr{W}_{ij}\left(\{\overline{U}_{g,l}\}\right)$ be the 2D reconstruction operator on the cell I_{ij}.

The reconstruction operator $\mathscr{W}_j(\cdot)$ (or the 2D version $\mathscr{W}_{ij}(\cdot)$) is said to be average-value-preserving if the reconstructed polynomial $U(x)$ satisfies

$$\sum_\alpha \omega_\alpha U(x_j^\alpha) = \overline{U}_j, \qquad \text{i.e.,} \qquad \mathscr{L}_j\left(\mathscr{W}_j\left(\{\overline{U}_l\}\right)\right) = \overline{U}_j, \ \text{ or } \ \mathscr{R}_j\left(\mathscr{W}_j\left(\{\overline{U}_l\}\right)\right) = \overline{U}_j,$$

where α can be either ν or κ referring to the Gauss-Lobatto or Romberg's quadrature.

In this paper, the modified WENO-ZQ reconstruction discussed in Section 2.4 is used in the WENO reconstruction operators $\mathscr{W}_j(\cdot)$ and $\mathscr{W}_{ij}(\cdot)$. This operator satisfies the average-value-preserving property, which can be easily observed from the reconstructed polynomial (2.18) and sufficient quadrature nodes. If the traditional WENO-JS reconstruction is used, only point values $U(x_j^\nu)$ are reconstructed, and one cannot obtain a polynomial on the cell I_j similar to (2.18). As such, the traditional WENO-JS reconstruction is generally not average-value-preserving and $\mathscr{L}_j\left(\mathscr{W}_j(\{\overline{U}_l\})\right) \neq \overline{U}_j$, which has been verified numerically.

Note that, in the FV framework, the WENO reconstruction with the average-value-preserving property is needed in the theoretical analysis of the PP property. See Sections 4-6. If only the well-balancedness is considered, any WENO-type reconstruction is feasible.

For references, we list some commonly used notations and variables in Table 3.1, in which all quantities are at the current nth time level unless otherwise specified.

3.2. Major conclusions

The general semidiscrete FV WENO method for the Euler model takes the form (2.8) or (2.12), where the choice of numerical fluxes and the corresponding source term discretization has not been specified. One key component in the design of

various PP and WB methods, including `New-WB`, `GLK-WB`, `KPS-WB` methods, is the reconstruction of cell interface values to be used in the computation of numerical fluxes. For these three WB methods, this procedure to reconstruct the polynomial $\mathbf{U}_j(x) = (\rho_j(x), m_j(x), E_j(x))^\top$ from cell averages is different, as different techniques were proposed to achieve WB property, and these will be described in detail in Sections 4-6.

Here we summarize the main theorems on PP properties, which show that schemes (2.9) and (2.13) have PP properties under certain conditions. These results hold for all three WB methods, to be discussed in the following sections.

Theorem 3.1 *(PP property of 1D method). Let $\mathbf{U}_j(x) = (\rho_j(x), m_j(x), E_j(x))^\top$ be the reconstructed function at the nth time level. For the 1D scheme (2.9) with numerical fluxes and source term to be specified in Sections 4-6, if*

$$\mathbf{U}_j(x) \in G, \quad x \in \mathbb{S}_j, \tag{3.19}$$

then $\overline{\mathbf{U}}_j^{n+1} \in G$ under the CFL-type condition

$$\widetilde{\alpha}_j \frac{\Delta t}{\Delta x} \le \omega_1, \tag{3.20}$$

where ω_1 is the first weight of the adopted numerical quadrature, and $\widetilde{\alpha}_j$ is a parameter to be determined for each method.

The proof of Theorem 3.1 is different for three WB methods due to different choices of numerical fluxes and source term approximation utilized. The detailed proof and the parameter $\widetilde{\alpha}_j$ will be presented in Section 4.1.2, Section 5.1.2 and Section 6.1.2, respectively.

Theorem 3.2 *(PP property of 2D method). Let $\mathbf{U}_{ij}(\mathbf{x}) = (\rho_{ij}(\mathbf{x}), \mathbf{m}_{ij}(\mathbf{x}), E_{ij}(\mathbf{x}))$ be the reconstructed function at the nth time level. For the 2D scheme (2.13) with numerical fluxes and source term to be specified in Sections 4-6, if*

$$\mathbf{U}_{ij}(\mathbf{x}) \in G, \quad \forall \mathbf{x} \in \mathbb{S}_{ij}, \tag{3.21}$$

then $\overline{\mathbf{U}}_{ij}^{n+1} \in G$ under the CFL-type condition

$$\Delta t \widetilde{\alpha}_{ij} \left(\frac{1}{\Delta x} + \frac{1}{\Delta y} \right) \le \omega_1, \tag{3.22}$$

where ω_1 is the first weight of the adopted numerical quadrature, and $\widetilde{\alpha}_{ij}$ is a parameter to be determined for each method.

The proof of Theorem 3.2 and the parameter $\widetilde{\alpha}_{ij}$ will be presented in Section 4.2.2, Section 5.2.2 and Section 6.2.2 for each method, respectively.

Theorems 3.1 and 3.2 give a sufficient condition for the PP property of numerical schemes if the forward Euler time discretization is applied. High-order SSP-RK time discretization (2.14) can be viewed as a convex combination of the forward Euler method. Therefore, according to Lemma 2.1, the conclusion of Theorems 3.1 and 3.2 also holds if the SSP-RK time discretization is used.

Remark 3.1. As shown in Theorem 3.1 and Theorem 3.2, both CFL-type conditions (3.20) and (3.22) are sufficient, but may not be necessary, for the sake of preserving the positivity of cell averages. To evolve numerical solutions at $(n+1)$th time level, we can start with a larger CFL number at the nth time level to save computational cost. If negative cell averages emerge in any of the three stages in one step of the third-order SSP RK method, we return to stage one and restart the computation with half the time size. The specific flowchart can refer to Section 3.3 in [5].

3.3. PP limiter

In general, given the set $\overline{\mathbf{U}}_j^n \in G$, the reconstructed function $\mathbf{U}(\mathbf{x})$ may not necessarily satisfy the condition (3.19) or (3.21). To enforce the condition (3.19) in Theorem 3.1 and (3.21) in Theorem 3.2, we present the following PP limiter [49–51] and take the 1D case as an example to present it.

We assume the reconstructed function $\mathbf{U}_j(x) = (\rho_j(x), m_j(x), E_j(x))^\top$ on the cell I_j with the cell average $\overline{\mathbf{U}}_j = (\overline{\rho}_j, \overline{m}_j, \overline{E}_j)$ and $\overline{\rho}_j, \rho e(\overline{\mathbf{U}}_j) > 0$. We use the following PP limiting procedure to modify $\mathbf{U}_j(x)$ into $\widetilde{\mathbf{U}}_j(x)$, so that $\widetilde{\mathbf{U}}_j(x) \in G$, for $x \in \mathbb{S}_j$.

1. Set a small number $\varepsilon_0 = \min_j\{10^{-13}, \overline{\rho}_j, \rho e(\overline{\mathbf{U}}_j)\}$. Evaluate $\theta_1 = \min\{|\frac{\overline{\rho}_j - \varepsilon_0}{\overline{\rho}_j - \min_{x \in \mathbb{S}_j} \rho_j(x)}|, 1\}$ in each cell I_j.
2. Modify the density by

$$\widehat{\rho}_j(x) = \theta_1(\rho_j(x) - \overline{\rho}_j) + \overline{\rho}_j.$$

3. Set $\widehat{\mathbf{U}}_j(x) = (\widehat{\rho}_j(x), m_j(x), E_j(x))$. To enforce the positivity of the internal energy, we perform the following procedure

$$\widetilde{\mathbf{U}}_j(x) = \theta_2(\widehat{\mathbf{U}}_j(x) - \overline{\mathbf{U}}_j) + \overline{\mathbf{U}}_j, \qquad \theta_2 = \min\left\{ \frac{\rho e(\overline{\mathbf{U}}_j) - \varepsilon_0}{\rho e(\overline{\mathbf{U}}_j) - \min\limits_{x\in\mathbb{S}_j} \rho e(\widehat{\mathbf{U}}_j(x))}, 1 \right\}.$$

4. In the numerical scheme (2.9), use $\widetilde{\mathbf{U}}_j(x)$ instead of $\mathbf{U}_j(x)$, which satisfies $\widetilde{\mathbf{U}}_j(x) \in G$, for $x \in \mathbb{S}_j$.

In fact, the complete expression of functions $\mathbf{U}_j(x)$ is not required, and we just need to modify these values at the points belonging to the set $\mathbb{S}_j$ according to the above PP limiter. A similar process can be applied to the reconstructed function $\mathbf{U}_{ij}(\mathbf{x})$ in the 2D case, by simply replacing the set $\mathbb{S}_j$ with $\mathbb{S}_{ij}$.

In the following sections (Sections 4-6), we will introduce numerical fluxes and discretization of the source term, and provide the proof of Theorem 3.1 and Theorem 3.2, for each of the three WB methods respectively.

4. `New-WB`: a new PPWB finite volume method

In this section, we construct a uniformly high-order FV PP WB WENO method (`New-WB` method), and present the rigorous analyses of its PP and WB properties.

4.1. One-dimensional `New-WB` scheme

4.1.1. WB numerical fluxes and source term discretization

Consider 1D Euler equations (2.6) with a general EoS $e = \mathscr{E}(\rho, p)$. The general semidiscrete finite volume WENO method takes the form (2.8), coupled with the modified WENO-ZQ reconstruction discussed in Section 2.4. Here we present WB numerical fluxes and the corresponding source term discretization.

The standard HLLC flux is a modified version of the HLL flux [29], and can be found in [2,29]. It is chosen here due to its contact property [6,37] (e.g. Lemma 4.1), which makes it easier to design WB methods. In order to achieve the WB property for general stationary hydrostatic solutions (2.2), we propose to modify the standard HLLC flux as

$$\widehat{\mathbf{F}}_{j+\frac{1}{2}} = \mathscr{F}^{hllc}\left(\frac{\rho^{e,-}_{j+\frac{1}{2}} e^{\star,-}_{j+\frac{1}{2}}}{(\rho e)^{e,-}_{j+\frac{1}{2}}} \mathbf{U}^{-}_{j+\frac{1}{2}}, \frac{\rho^{e,+}_{j+\frac{1}{2}} e^{\star,+}_{j+\frac{1}{2}}}{(\rho e)^{e,+}_{j+\frac{1}{2}}} \mathbf{U}^{+}_{j+\frac{1}{2}} \right) \tag{4.1}$$

with the quantity $\mathbf{U}^{\mp}_{j\pm\frac{1}{2}}$ computed by $\mathscr{W}_j(\{\overline{\mathbf{U}}_l\})$, and

$$e^{\star,\pm}_{j+\frac{1}{2}} := \mathscr{E}\left(\rho^{e,\pm}_{j+\frac{1}{2}}, p^{e,\star}_{j+\frac{1}{2}}\right),$$

where $p^{e,\star}_{j+\frac{1}{2}}$ is an approximation to the equilibrium pressure at interface $x_{j+\frac{1}{2}}$, defined by

$$p^{e,\star}_{j+\frac{1}{2}} = \frac{1}{2}\left(p^{e,-}_{j+\frac{1}{2}} + p^{e,+}_{j+\frac{1}{2}}\right). \tag{4.2}$$

Above mentioned values at the interface can be obtained by the modified WENO-ZQ reconstruction. This modification to the HLLC flux will not destroy the high-order accuracy of the numerical scheme if both $\rho^e(x)$ and $p^e(x)$ are smooth [37].

The WB approximation of the source term follows the technique in [23,24,41]. The integral of the source term in the momentum equation can be decomposed into

$$\begin{aligned} \frac{1}{\Delta x}\int_{I_j} S^{[2]}\mathrm{d}x &= \frac{1}{\Delta x}\int_{I_j} -\rho\phi_x \mathrm{d}x = \frac{1}{\Delta x}\int_{I_j} \frac{\rho}{\rho^e} p^e_x \mathrm{d}x = \frac{1}{\Delta x}\int_{I_j} \left(\frac{\rho}{\rho^e} - \frac{\overline{\rho}_j}{\overline{\rho}^e_j} + \frac{\overline{\rho}_j}{\overline{\rho}^e_j}\right) p^e_x \mathrm{d}x \\ &= \frac{1}{\Delta x}\int_{I_j} \left(\frac{\rho}{\rho^e} - \frac{\overline{\rho}_j}{\overline{\rho}^e_j}\right) p^e_x \mathrm{d}x + \frac{1}{\Delta x}\frac{\overline{\rho}_j}{\overline{\rho}^e_j}\left(p^{e,-}_{j+\frac{1}{2}} - p^{e,+}_{j-\frac{1}{2}}\right). \end{aligned} \tag{4.3}$$

This motivates us to employ the following numerical approximation

$$\overline{S}^{[2]}_j := \mathscr{L}_j\left(\left(\frac{\rho}{\rho^e} - \frac{\overline{\rho}_j}{\overline{\rho}^e_j}\right) p^e_x\right) + \frac{1}{\Delta x}\frac{\overline{\rho}_j}{\overline{\rho}^e_j}\left(p^{e,\star}_{j+\frac{1}{2}} - p^{e,\star}_{j-\frac{1}{2}}\right) = \mathscr{L}_j\left(\frac{\rho}{\rho^e} p^e_x\right) + \frac{\overline{\rho}_j}{\overline{\rho}^e_j}\tau, \tag{4.4}$$

where

$$\tau = \frac{1}{\Delta x}\left(p^{e,\star}_{j+\frac{1}{2}} - p^{e,\star}_{j-\frac{1}{2}}\right) - \mathscr{L}_j\left(p^e_x\right) \tag{4.5}$$

is the WB correction term. Similarly, the integral of the source term in the energy equation can be approximated by

$$\overline{S}^{[3]}_j := \mathscr{L}_j\left(\frac{m}{\rho^e}p^e_x\right) + \frac{\overline{m}_j}{\overline{\rho}^e_j}\tau. \tag{4.6}$$

The combination of (2.8), (4.1), (4.4), and (4.6) yields the `New-WB` WENO method for Euler equations (2.6).

Remark 4.1. As mentioned in [37, Remark 3.2], it is necessary to use the numerical approximation (4.6) for $\overline{S}^{[3]}_j$, which is consistent with (4.4) for $\overline{S}^{[2]}_j$, in order to accommodate the analysis of the PP property.

Now, we are ready to prove the WB property of the proposed `New-WB` method. As mentioned in [37], the contact property [6] of HLLC flux can also be extended to the general EoS case, which can be described as Lemma 4.1.

Lemma 4.1. *For any two equilibrium states* $\mathbf{U}_L = \left(\rho_L, 0, \rho_L\mathscr{E}(\rho_L, p)\right)^\top$ *and* $\mathbf{U}_R = \left(\rho_R, 0, \rho_R\mathscr{E}(\rho_R, p)\right)^\top$*, the 1D HLLC flux* (4.1) *satisfies*

$$\mathscr{F}^{hllc}(\mathbf{U}_L, \mathbf{U}_R) = (0, p, 0)^\top.$$

Theorem 4.1. *For 1D Euler equations* (2.6)*, the* `New-WB` *method is WB for the stationary hydrostatic solutions* (2.2)*.*

Proof. At the equilibrium state, we have $\overline{\rho} = \overline{\rho}^e$, $\overline{u} = \overline{u}^e = 0$ and $\overline{\rho e} = \overline{(\rho e)}^e$ which leads to

$$\frac{\rho^{e,\pm}_{j+\frac{1}{2}} e^{\star,\pm}_{j+\frac{1}{2}}}{(\rho e)^{e,\pm}_{j+\frac{1}{2}}}\mathbf{U}^{\pm}_{j+\frac{1}{2}} = \left(\rho^{e,\pm}_{j+\frac{1}{2}}\frac{\rho^{e,\pm}_{j+\frac{1}{2}} e^{\star,\pm}_{j+\frac{1}{2}}}{(\rho e)^{e,\pm}_{j+\frac{1}{2}}}, 0, \rho^{e,\pm}_{j+\frac{1}{2}} e^{\star,\pm}_{j+\frac{1}{2}}\right).$$

According to Lemma 4.1, the modified HLLC flux becomes

$$\widehat{\mathbf{F}}_{j+\frac{1}{2}} = \left(0,\ p^{e,\star}_{j+\frac{1}{2}},\ 0\right)^\top. \tag{4.7}$$

On the other hand, the source term approximation $\overline{S}^{[3]}_j = 0$, and $\overline{S}^{[2]}_j$ reduces to

$$\overline{S}^{[2]}_j = \frac{1}{\Delta x}\left(p^{e,\star}_{j+\frac{1}{2}} - p^{e,\star}_{j-\frac{1}{2}}\right),$$

since $\frac{\rho(x^\nu_j)}{\rho^e(x^\nu_j)} = \frac{\overline{\rho}_j}{\overline{\rho}^e_j} = 1$. The second element of $\mathbf{F}(\mathbf{U})$ reduces to p due to $u = 0$, and according to (4.7), we have

$$\frac{1}{\Delta x}\left(\widehat{\mathbf{F}}^{[2]}_{j+\frac{1}{2}} - \widehat{\mathbf{F}}^{[2]}_{j-\frac{1}{2}}\right) = \frac{1}{\Delta x}\left(p^{e,\star}_{j+\frac{1}{2}} - p^{e,\star}_{j-\frac{1}{2}}\right),$$

where $\widehat{\mathbf{F}}^{[2]}_{j+\frac{1}{2}}$ stands for the second element of $\widehat{\mathbf{F}}_{j+\frac{1}{2}}$. Therefore, the numerical flux and source term of the momentum equation balance exactly. In addition, the numerical flux and source term both reduce to 0 for the density and energy equations, which implies the WB property of the proposed `New-WB` scheme. □

4.1.2. Analysis of PP property

In this subsection, we study the PP property of the proposed `New-WB` scheme. Before that, we present two Lemmas of the HLLC flux studied in [37].

Lemma 4.2. *Given two admissible states* $\mathbf{U}_0, \mathbf{U}_1 \in G$*, one has*

$$\mathbf{U}_0 - \lambda\left(\mathscr{F}^{hllc}(\mathbf{U}_0, \mathbf{U}_1) - \mathbf{F}(\mathbf{U}_0)\right) \in G, \tag{4.8}$$

$$\mathbf{U}_1 - \lambda\left(\mathbf{F}(\mathbf{U}_1) - \mathscr{F}^{hllc}(\mathbf{U}_0, \mathbf{U}_1)\right) \in G, \tag{4.9}$$

if $\lambda \in \mathbb{R}^+$ *satisfies*

$$\lambda \max_{\mathbf{U}\in\{\mathbf{U}_0,\mathbf{U}_1\}} \alpha_{\max}(\mathbf{U}) \le 1 \tag{4.10}$$

with

$$\alpha_{\max}(\mathbf{U}) := |u| + \hat{c}, \qquad \textit{and} \quad \hat{c} = \frac{p}{\rho\sqrt{2e}}. \tag{4.11}$$

Lemma 4.3. *For any parameters $\mu_L,\ \mu_M,\ \mu_R \in \mathbb{R}^+$ and any admissible states $\mathbf{U}_L, \mathbf{U}_M, \mathbf{U}_R \in G$, we have*

$$\mu_M\mathbf{U}_M - \lambda\left(\mathscr{F}^{hllc}(\mu_M\mathbf{U}_M, \mu_R\mathbf{U}_R) - \mathscr{F}^{hllc}(\mu_L\mathbf{U}_L, \mu_M\mathbf{U}_M)\right) \in G,$$

if $\lambda \in \mathbb{R}^+$ satisfies

$$\lambda \max_{\mathbf{U}\in\{\mathbf{U}_L,\mathbf{U}_M,\mathbf{U}_R\}} \alpha_{\max}(\mathbf{U}) \le \frac{1}{2}. \tag{4.12}$$

Theorem 3.1 on PP property holds for the 1D `New-WB` scheme, with the parameter $\widetilde{\alpha}_j := \widetilde{\alpha}_j^F + \widetilde{\alpha}_j^{S_1} + \widetilde{\alpha}_j^{S_2}$ defined by

$$\widetilde{\alpha}_j^F := 2\max\left\{\frac{\rho^{e,-}_{j+\frac12}e^{\star,-}_{j+\frac12}}{(\rho e)^{e,-}_{j+\frac12}}, \frac{\rho^{e,+}_{j-\frac12}e^{\star,+}_{j-\frac12}}{(\rho e)^{e,+}_{j-\frac12}}\right\} \max_{\mathbf{U}\in\{\mathbf{U}^{\pm}_{j-\frac12},\mathbf{U}^{\pm}_{j+\frac12}\}} \alpha_{\max}(\mathbf{U}), \tag{4.13a}$$

$$\widetilde{\alpha}_j^{S_1} := \omega_1\Delta x \max_{1\le\nu\le L}\left\{\frac{\left|p^e_x(x_j^\nu)\right|}{\rho^e(x_j^\nu)\sqrt{2e(x_j^\nu)}}\right\}, \qquad \widetilde{\alpha}_j^{S_2} := \omega_1\Delta x\frac{|\tau|}{\overline{\rho}^e_j\sqrt{2\overline{e}_j}}, \tag{4.13b}$$

respectively. Here $\widetilde{\alpha}_j^{S_1} + \widetilde{\alpha}_j^{S_2} = \mathscr{O}(\Delta x)$ and $\max\left\{\frac{\rho^{e,-}_{j+\frac12}e^{\star,-}_{j+\frac12}}{(\rho e)^{e,-}_{j+\frac12}}, \frac{\rho^{e,+}_{j-\frac12}e^{\star,+}_{j-\frac12}}{(\rho e)^{e,+}_{j-\frac12}}\right\} = 1 + \mathscr{O}(\Delta x^{k+1})$ for smooth $\rho^e(x), e^e(x)$. The proof of Theorem 3.1 for the `New-WB` method is presented below.

Proof. Since the proof is long and part of it can be reused in the following sections, we decompose the proof into the following five steps:

Step 1: Decomposition. Based on the 1D scheme (2.9), we introduce a suitable parameter $\eta \in (0, 1]$ whose value will be determined later, and consider the following decomposition

$$\begin{aligned}
\overline{\mathbf{U}}_j^{n+1} &= \overline{\mathbf{U}}_j^n + \Delta t\mathbf{L}_j(\overline{\mathbf{U}}^n) = \eta\overline{\mathbf{U}}_j^n - \frac{\Delta t}{\Delta x}\left(\widehat{\mathbf{F}}_{j+\frac12} - \widehat{\mathbf{F}}_{j-\frac12}\right) + (1-\eta)\overline{\mathbf{U}}_j^n + \Delta t\overline{\mathbf{S}}_j \\
&= \left[\eta\overline{\mathbf{U}}_j^n - \eta\omega_1\left(\mathbf{U}^+_{j-\frac12} + \mathbf{U}^-_{j+\frac12}\right)\right] + \left[\eta\omega_1\left(\mathbf{U}^+_{j-\frac12} + \mathbf{U}^-_{j+\frac12}\right) - \frac{\Delta t}{\Delta x}\left(\widehat{\mathbf{F}}_{j+\frac12} - \widehat{\mathbf{F}}_{j-\frac12}\right)\right] \\
&\quad + \left[(1-\eta)\overline{\mathbf{U}}_j^n + \Delta t\overline{\mathbf{S}}_j\right] =: \mathbf{W}_1 + \mathbf{W}_2 + \mathbf{W}_3.
\end{aligned} \tag{4.14}$$

Next we need to prove that $\mathbf{W}_1$, $\mathbf{W}_2$ and $\mathbf{W}_3$ are in the set G and also select the suitable choice of the parameter η, which are presented in Steps 2-5 below.

Step 2: $\mathbf{W}_1 \in G$. Recall that $\mathbf{W}_1 := \eta\overline{\mathbf{U}}_j^n - \eta\omega_1\left(\mathbf{U}^+_{j-\frac12} + \mathbf{U}^-_{j+\frac12}\right)$. Following the discussions in Section 3.1, we have the following formulation for the WENO reconstruction polynomial $U_j(x)$ (obtained from $\{\overline{U}_l\}$) in the cell I_j:

$$\overline{\mathbf{U}}_j = \mathscr{L}_j\left(\mathscr{W}_j(\{\overline{U}_l\})\right) = \sum_{\nu=1}^{L}\omega_\nu\mathbf{U}(x_j^\nu). \tag{4.15}$$

Hence, from the assumption (3.19) and Lemma 2.1, we can easily obtain

$$\mathbf{W}_1 = \eta\sum_{\nu=2}^{L-1}\omega_\nu\mathbf{U}(x_j^\nu) \in G. \tag{4.16}$$

Step 3: $\mathbf{W}_2 \in G$. Let's consider the term $\mathbf{W}_2 := \eta\omega_1\left(\mathbf{U}^+_{j-\frac12} + \mathbf{U}^-_{j+\frac12}\right) - \frac{\Delta t}{\Delta x}\left(\widehat{\mathbf{F}}_{j+\frac12} - \widehat{\mathbf{F}}_{j-\frac12}\right)$, which can be decomposed into

$$\begin{aligned}
\mathbf{W}_2 &= \eta\omega_1\mathbf{U}^+_{j-\frac12} + \eta\omega_1\mathbf{U}^-_{j+\frac12} \\
&\quad - \frac{\Delta t}{\Delta x}\left[\mathscr{F}^{hllc}\left(\frac{\rho^{e,-}_{j+\frac12}e^{\star,-}_{j+\frac12}}{(\rho e)^{e,-}_{j+\frac12}}\mathbf{U}^-_{j+\frac12}, \frac{\rho^{e,+}_{j+\frac12}e^{\star,+}_{j+\frac12}}{(\rho e)^{e,+}_{j+\frac12}}\mathbf{U}^+_{j+\frac12}\right) - \mathscr{F}^{hllc}\left(\frac{\rho^{e,-}_{j-\frac12}e^{\star,-}_{j-\frac12}}{(\rho e)^{e,-}_{j-\frac12}}\mathbf{U}^-_{j-\frac12}, \frac{\rho^{e,+}_{j-\frac12}e^{\star,+}_{j-\frac12}}{(\rho e)^{e,+}_{j-\frac12}}\mathbf{U}^+_{j-\frac12}\right)\right]
\end{aligned}$$

$$=: \eta\omega_1 \frac{(\rho e)^{e,-}_{j+\frac{1}{2}}}{\rho^{e,-}_{j+\frac{1}{2}} e^{\star,-}_{j+\frac{1}{2}}} \mathbf{W}_2^+ + \eta\omega_1 \frac{(\rho e)^{e,+}_{j-\frac{1}{2}}}{\rho^{e,+}_{j-\frac{1}{2}} e^{\star,+}_{j-\frac{1}{2}}} \mathbf{W}_2^-,$$

where

$$\begin{aligned}
\mathbf{W}_2^+ &= \frac{\rho^{e,-}_{j+\frac{1}{2}} e^{\star,-}_{j+\frac{1}{2}}}{(\rho e)^{e,-}_{j+\frac{1}{2}}} \mathbf{U}^-_{j+\frac{1}{2}} - \frac{\Delta t}{\eta\omega_1 \Delta x} \frac{\rho^{e,-}_{j+\frac{1}{2}} e^{\star,-}_{j+\frac{1}{2}}}{(\rho e)^{e,-}_{j+\frac{1}{2}}} \\
&\quad \times \left[\mathscr{F}^{hllc}\left(\frac{\rho^{e,-}_{j+\frac{1}{2}} e^{\star,-}_{j+\frac{1}{2}}}{(\rho e)^{e,-}_{j+\frac{1}{2}}} \mathbf{U}^-_{j+\frac{1}{2}}, \frac{\rho^{e,+}_{j+\frac{1}{2}} e^{\star,+}_{j+\frac{1}{2}}}{(\rho e)^{e,+}_{j+\frac{1}{2}}} \mathbf{U}^+_{j+\frac{1}{2}} \right) - \mathscr{F}^{hllc}\left(\frac{\rho^{e,+}_{j-\frac{1}{2}} e^{\star,+}_{j-\frac{1}{2}}}{(\rho e)^{e,+}_{j-\frac{1}{2}}} \mathbf{U}^+_{j-\frac{1}{2}}, \frac{\rho^{e,-}_{j+\frac{1}{2}} e^{\star,-}_{j+\frac{1}{2}}}{(\rho e)^{e,-}_{j+\frac{1}{2}}} \mathbf{U}^-_{j+\frac{1}{2}} \right) \right], \\
\mathbf{W}_2^- &= \frac{\rho^{e,+}_{j-\frac{1}{2}} e^{\star,+}_{j-\frac{1}{2}}}{(\rho e)^{e,+}_{j-\frac{1}{2}}} \mathbf{U}^+_{j-\frac{1}{2}} - \frac{\Delta t}{\eta\omega_1 \Delta x} \frac{\rho^{e,+}_{j-\frac{1}{2}} e^{\star,+}_{j-\frac{1}{2}}}{(\rho e)^{e,+}_{j-\frac{1}{2}}} \\
&\quad \times \left[\mathscr{F}^{hllc}\left(\frac{\rho^{e,+}_{j-\frac{1}{2}} e^{\star,+}_{j-\frac{1}{2}}}{(\rho e)^{e,+}_{j-\frac{1}{2}}} \mathbf{U}^+_{j-\frac{1}{2}}, \frac{\rho^{e,-}_{j+\frac{1}{2}} e^{\star,-}_{j+\frac{1}{2}}}{(\rho e)^{e,-}_{j+\frac{1}{2}}} \mathbf{U}^-_{j+\frac{1}{2}} \right) - \mathscr{F}^{hllc}\left(\frac{\rho^{e,-}_{j-\frac{1}{2}} e^{\star,-}_{j-\frac{1}{2}}}{(\rho e)^{e,-}_{j-\frac{1}{2}}} \mathbf{U}^-_{j-\frac{1}{2}}, \frac{\rho^{e,+}_{j-\frac{1}{2}} e^{\star,+}_{j-\frac{1}{2}}}{(\rho e)^{e,+}_{j-\frac{1}{2}}} \mathbf{U}^+_{j-\frac{1}{2}} \right) \right].
\end{aligned}$$

Thanks to the assumption (3.19) and Lemma 4.3, we have $\mathbf{W}_2^{\pm} \in G$, if

$$\Delta t \widetilde{\alpha}_j^F \le \eta\omega_1 \Delta x, \tag{4.17}$$

where $\widetilde{\alpha}_j^F$ is defined in (4.13), and $\alpha_{\max}(\mathbf{U})$ is defined by (4.11).

Step 4: $\mathbf{W}_3 \in G$. Now we consider the term $\mathbf{W}_3 := (1-\eta)\overline{\mathbf{U}}_j^n + \Delta t \overline{\mathbf{S}}_j$. For any parameter $\lambda \in [0,1]$, we have

$$\begin{aligned}
(1-\eta)\overline{m}_j + \Delta t \overline{S}_j^{[2]} &= (1-\eta)\lambda \mathscr{L}_j(m(x)) + (1-\eta)(1-\lambda)\overline{m}_j + \Delta t \left(\mathscr{L}_j\left(\frac{\rho}{\rho^e} p_x^e \right) + \frac{\overline{\rho}_j}{\overline{\rho}_j^e} \tau \right), \\
(1-\eta)\overline{E}_j + \Delta t \overline{S}_j^{[3]} &= (1-\eta)\lambda \mathscr{L}_j(E(x)) + (1-\eta)(1-\lambda)\overline{E}_j + \Delta t \left(\mathscr{L}_j\left(\frac{m}{\rho^e} p_x^e \right) + \frac{\overline{m}_j}{\overline{\rho}_j^e} \tau \right).
\end{aligned}$$

Therefore, we have

$$\mathbf{W}_3 = \sum_{\nu=1}^{L} \omega_\nu \left[(1-\eta)\lambda \mathbf{U}(x_j^\nu) + \frac{\Delta t (p^e)_x(x_j^\nu)}{\rho^e(x_j^\nu)} \begin{pmatrix} 0 \\ \rho(x_j^\nu) \\ m(x_j^\nu) \end{pmatrix} \right] + (1-\eta)(1-\lambda)\overline{\mathbf{U}}_j + \frac{\Delta t}{\overline{\rho}_j^e} \begin{pmatrix} 0 \\ \overline{\rho}_j \tau \\ \overline{m}_j \tau \end{pmatrix}. \tag{4.18}$$

Following Lemma 2.1 and Lemma 2.2, we can obtain $\mathbf{W}_3 \in G$ if

$$\Delta t \widetilde{\alpha}_j^{S_1} \le \omega_1 \Delta x (1-\eta)\lambda, \qquad \Delta t \widetilde{\alpha}_j^{S_2} \le \omega_1 \Delta x (1-\eta)(1-\lambda), \tag{4.19}$$

with $\alpha_j^{S_1}$ and $\alpha_j^{S_2}$ defined in (4.13).

Combining Steps 1-4, we conclude that if Δt satisfies

$$\Delta t \in \Omega_{\eta,\lambda}^{(j)} := \left\{ s \in \mathbb{R}^+ : \ s\widetilde{\alpha}_j^F \le \eta\omega_1 \Delta x, \ \ s\widetilde{\alpha}_j^{S_1} \le \omega_1 \Delta x (1-\eta)\lambda, \ \ s\widetilde{\alpha}_j^{S_2} \le \omega_1 \Delta x (1-\eta)(1-\lambda) \right\}, \tag{4.20}$$

then $\overline{\mathbf{U}}_j^{n+1} \in G$ following Lemma 2.1.

Step 5: "optimal" parameters. Let $g(\eta,\lambda) := \sup \Omega_{\eta,\lambda}^{(j)}$, the condition (4.20) is equivalent to $\Delta t \le g(\eta,\lambda)$, for any $\eta, \lambda \in (0,1]$. This implies that we need to determine an optimal value s^* ($s^* = \max(s)$) such that

$$s^* = \min(A, B, C),$$

where $A = \frac{\eta\omega_1 \Delta x}{\widetilde{\alpha}_j^F}$, $B = \frac{\omega_1 \Delta x (1-\eta)\lambda}{\widetilde{\alpha}_j^{S_1}}$ and $C = \frac{\omega_1 \Delta x (1-\eta)(1-\lambda)}{\widetilde{\alpha}_j^{S_2}}$. By setting $A = B = C$, we can obtain two "optimal" parameters

$$\eta = \eta^* = \frac{\widetilde{\alpha}_j^F}{\widetilde{\alpha}_j} \text{ and } \lambda = \lambda^* = \frac{\widetilde{\alpha}_j^{S_1}}{\widetilde{\alpha}_j^{S_1} + \widetilde{\alpha}_j^{S_2}}, \tag{4.21}$$

such that

$$\max_{\eta\in(0,1],\lambda\in[0,1]} g(\eta,\lambda)=g(\eta^*,\lambda^*)=\frac{\omega_1\Delta x}{\widetilde{\alpha}_j^F+\widetilde{\alpha}_j^{S_1}+\widetilde{\alpha}_j^{S_2}}=\frac{\omega_1\Delta x}{\widetilde{\alpha}_j}.$$

Therefore, the condition (4.20) reduces to

$$\Delta t\le g(\eta^*,\lambda^*)=\frac{\omega_1\Delta x}{\widetilde{\alpha}_j}$$

which is equivalent to (3.20). This finishes the proof. □

Remark 4.2. Note that, in a special case when $\left\{\frac{(p^e)_x(x_j^\nu)}{\rho^e(x_j^\nu)}\right\}_{\nu=1}^{L}\equiv\mathbb{C}$ in each cell I_j (for example, the isothermal hydrostatic state in Section 2.1), Theorem 3.1 can be proven with a simpler condition

$$\frac{\overline{\mathbf{U}}_j-\omega_1(\mathbf{U}^+_{j-\frac12}+\mathbf{U}^-_{j+\frac12})}{1-2\omega_1}\in G,\quad\text{and}\quad\mathbf{U}^\mp_{j\pm\frac12}\in G,\tag{4.22}$$

instead of (3.19). Under such condition, $\mathbf{W}_1\in G$ in (4.16) holds. The proof of $\mathbf{W}_2\in G$ is the same. For the term $\mathbf{W}_3$, we can decompose the first term of the right-hand side in (4.18) as:

$$(1-\eta)\lambda\sum_{\nu=1}^{L}\omega_\nu\mathbf{U}(x_j^\nu)+\Delta t\sum_{\nu=1}^{L}\omega_\nu\frac{(p^e)_x(x_j^\nu)}{\rho^e(x_j^\nu)}\left(0,\ \rho(x_j^\nu),\ m(x_j^\nu)\right)^\top:=W_{31}+W_{32}.$$

According to [40,48], there exist some points x_j^1,x_j^2,x_j^3 in the cell I_j such that

$$\mathbf{U}_j^*:=\left(\rho(x_j^1),m(x_j^2),E(x_j^3)\right)=\frac{\overline{\mathbf{U}}_j-\omega_1(\mathbf{U}^+_{j-\frac12}+\mathbf{U}^-_{j+\frac12})}{1-2\omega_1}.\tag{4.23}$$

Therefore, W_{31} and W_{32} can be rewritten as

$$W_{31}=(1-\eta)\lambda[\omega_1(\mathbf{U}^+_{j-\frac12}+\mathbf{U}^-_{j+\frac12})+(1-2\omega_1)\mathbf{U}_j^*],$$
$$W_{32}=\Delta t[\omega_1(\mathbf{Q}^+_{j-\frac12}+\mathbf{Q}^-_{j+\frac12})+(1-2\omega_1)\mathbf{Q}_j^*],$$

where $\mathbf{Q}=(0,\frac{\rho p_x^e}{\rho^e},\frac{mp_x^e}{\rho^e})^\top$. In case of $\left\{\frac{(p^e)_x(x_j^\nu)}{\rho^e(x_j^\nu)}\right\}_{\nu=1}^{L}\equiv\mathbb{C}$, we have $\mathbf{Q}=\mathbb{C}(0,\rho,m)^\top$, so that $\mathbf{W}_3\in G$ under the condition (4.22).

4.2. Two-dimensional `New-WB` scheme

4.2.1. WB numerical flux and source term discretization

Consider 2D Euler equations (2.10) with the general semidiscrete finite volume WENO method given by (2.12). WB numerical fluxes and the corresponding source term discretization will be presented. For 2D Euler equations, the modified WB HLLC fluxes are given by

$$\widehat{\mathbf{F}}_{i+\frac12,j}=\sum_\nu\omega_\nu\mathscr{F}^{hllc}\left(\frac{\rho^{e,-}_{i+\frac12,\nu}e^{\star,-}_{i+\frac12,\nu}}{(\rho e)^{e,-}_{i+\frac12,\nu}}\mathbf{U}^-_{i+\frac12,\nu},\frac{\rho^{e,+}_{i+\frac12,\nu}e^{\star,+}_{i+\frac12,\nu}}{(\rho e)^{e,+}_{i+\frac12,\nu}}\mathbf{U}^+_{i+\frac12,\nu}\right)=:\sum_\nu\omega_\nu\mathscr{F}^{hllc}{}_{i+\frac12,j},\tag{4.24}$$

$$\widehat{\mathbf{G}}_{i,j+\frac12}=\sum_\nu\omega_\nu\mathscr{G}^{hllc}\left(\frac{\rho^{e,-}_{\nu,j+\frac12}e^{\star,-}_{\nu,j+\frac12}}{(\rho e)^{e,-}_{\nu,j+\frac12}}\mathbf{U}^-_{\nu,j+\frac12},\frac{\rho^{e,+}_{\nu,j+\frac12}e^{\star,+}_{\nu,j+\frac12}}{(\rho e)^{e,+}_{\nu,j+\frac12}}\mathbf{U}^+_{\nu,j+\frac12}\right)=:\sum_\nu\omega_\nu\mathscr{G}^{hllc}{}_{i,j+\frac12},\tag{4.25}$$

where $\mathscr{F}^{hllc}$ and $\mathscr{G}^{hllc}$ is the standard HLLC flux, $e^{e,\pm}_{i+\frac12,\nu}=\mathscr{E}\left(\rho^e(x^\pm_{i+\frac12},y_j^\nu),p^e(x^\pm_{i+\frac12},y_j^\nu)\right)$, and

$$e^{\star,\pm}_{i+\frac12,\nu}=\mathscr{E}\left(\rho^e(x^\pm_{i+\frac12},y_j^\nu),p^{e,\star}(x_{i+\frac12},y_j^\nu)\right),\quad p^{e,\star}(x_{i+\frac12},y_j^\nu)=\frac12\left(p^e(x^-_{i+\frac12},y_j^\nu)+p^e(x^+_{i+\frac12},y_j^\nu)\right).$$

All the boundary values $\mathbf{U}^\pm_{i+\frac12,\nu}$, $\mathbf{U}^\pm_{\nu,j+\frac12}$ are obtained by the modified WENO-ZQ reconstruction.

Following the same WB technique for approximating source term integrals in the 1D case, we have

$$\overline{S}_{ij}^{[2]} = \mathscr{L}_{ij}(\frac{\rho}{\rho^e} p_x^e) + \frac{\overline{\rho}_{ij}}{\overline{\rho}_{ij}^e}\tau_x, \tag{4.26a}$$

$$\overline{S}_{ij}^{[3]} = \mathscr{L}_{ij}(\frac{\rho}{\rho^e} p_y^e) + \frac{\overline{\rho}_{ij}}{\overline{\rho}_{ij}^e}\tau_y, \tag{4.26b}$$

$$\overline{S}_{ij}^{[4]} = \mathscr{L}_{ij}(\frac{\mathbf{m}}{\rho^e}\cdot\nabla p^e) + \frac{\overline{\mathbf{m}}_{ij}}{\overline{\rho}_{ij}^e}\cdot\widetilde{\tau}, \tag{4.26c}$$

with the WB correction term $\widetilde{\tau} = (\tau_x, \tau_y)$ defined by

$$\begin{aligned}
\tau_x &= \frac{1}{\Delta x}\mathscr{L}_j\left(p^{e,\star}(x_{i+\frac{1}{2}}, y)\right) - \frac{1}{\Delta x}\mathscr{L}_j\left(p^{e,\star}(x_{i-\frac{1}{2}}, y)\right) - \mathscr{L}_{ij}(p_x^e),\\
\tau_y &= \frac{1}{\Delta y}\mathscr{L}_i\left(p^{e,\star}(x, y_{j+\frac{1}{2}})\right) - \frac{1}{\Delta y}\mathscr{L}_i\left(p^{e,\star}(x, y_{j-\frac{1}{2}})\right) - \mathscr{L}_{ij}(p_y^e).
\end{aligned} \tag{4.27}$$

Below we list the contact property of the HLLC flux and the WB property of the proposed method. The proof is similar to the 1D case and is omitted here.

Lemma 4.4. *For equilibrium states* $\mathbf{U}_L = \left(\rho_L, 0, 0, \rho_L\mathscr{E}(\rho_L, p)\right)^\top$ *and* $\mathbf{U}_R = \left(\rho_R, 0, 0, \rho_R\mathscr{E}(\rho_R, p)\right)^\top$, *the standard HLLC flux satisfies*

$$\mathscr{F}^{hllc}(\mathbf{U}_L, \mathbf{U}_R) = (0, p, 0, 0)^\top, \qquad \mathscr{G}^{hllc}(\mathbf{U}_L, \mathbf{U}_R) = (0, 0, p, 0)^\top.$$

Theorem 4.2. *For 2D Euler equations* (2.10), *the* `New-WB` *method is WB for the stationary solutions* (2.2).

4.2.2. Analysis of PP property

Let point sets $\{x_i^{\nu_1}\} = \{x_i^\nu\}$ be Gauss-Lobatto quadrature points with algebraic precision k in the cell $[x_{i-\frac{1}{2}}, x_{i+\frac{1}{2}}]$, and similarly, $\{y_j^{\nu_1}\} = \{y_j^\nu\}$. We have the following formulation for the WENO reconstruction polynomial $U_{ij}(x, y)$ (obtained from $\{\overline{U}_{g,l}\}$) in the cell I_{ij}:

$$\begin{aligned}
\overline{U}_{ij} &= \frac{\lambda_1}{\lambda_1+\lambda_2}\mathscr{L}_{ij}\left(\mathscr{W}_{ij}(\{\overline{U}_{g,l}\})\right) + \frac{\lambda_2}{\lambda_1+\lambda_2}\mathscr{L}_{ij}\left(\mathscr{W}_{ij}(\{\overline{U}_{g,l}\})\right)\\
&= \sum_{\nu=1}^{L}\omega_1\omega_\nu\left(\frac{\lambda_2}{\lambda_1+\lambda_2}\left(U_{ij}(x_i^\nu, y_{j-\frac{1}{2}}) + U_{ij}(x_i^\nu, y_{j+\frac{1}{2}})\right) + \frac{\lambda_1}{\lambda_1+\lambda_2}\left(U_{ij}(x_{i-\frac{1}{2}}, y_j^\nu) + U_{ij}(x_{i+\frac{1}{2}}, y_j^\nu)\right)\right)\\
&+ \sum_{\nu_1=2}^{L-1}\sum_{\nu=1}^{L}\omega_\nu\omega_{\nu_1}\left(\frac{\lambda_2}{\lambda_1+\lambda_2}U_{ij}(x_i^\nu, y_j^{\nu_1}) + \frac{\lambda_1}{\lambda_1+\lambda_2}\mathbf{U}_{ij}(x_i^{\nu_1}, y_j^\nu)\right).
\end{aligned} \tag{4.28}$$

According to the definition of the set of Gauss-Lobatto nodes in Section 3, we have

$$\sum_q \hat{\omega}_q U_{ij}(\mathbf{x}^q) = \sum_{\nu=1}^{L}\sum_{\nu_1=1}^{L}\omega_\nu\omega_{\nu_1}U_{ij}(x_i^\nu, y_j^{\nu_1}) = \sum_{\nu_1=1}^{L}\sum_{\nu=1}^{L}\omega_{\nu_1}\omega_\nu U_{ij}(x_i^{\nu_1}, y_j^\nu). \tag{4.29}$$

Theorem 3.2 on PP property holds for the 2D `New-WB` scheme, in which $\widetilde{\alpha}_{ij} := \widetilde{\alpha}_{ij}^F + \widetilde{\alpha}_{ij}^{S_1} + \widetilde{\alpha}_{ij}^{S_2}$ with

$$\widetilde{\alpha}_{ij}^F := 2\max_\nu\left\{\frac{\rho_{i\pm\frac{1}{2},\nu}^{e,\mp}e_{i\pm\frac{1}{2},\nu}^{\star,\mp}}{(\rho e)_{i\pm\frac{1}{2},\nu}^{e,\mp}}, \frac{\rho_{\nu,j\pm\frac{1}{2}}^{e,\mp}e_{\nu,j\pm\frac{1}{2}}^{\star,\mp}}{(\rho e)_{\nu,j\pm\frac{1}{2}}^{e,\mp}}\right\}\max_\nu\left\{\max_{\mathbf{U}\in\{\mathbf{U}_{i\pm\frac{1}{2},\nu}^\pm, \mathbf{U}_{\nu,j\pm\frac{1}{2}}^\pm\}}\alpha_{\max}(\mathbf{U})\right\}, \tag{4.30a}$$

$$\widetilde{\alpha}_{ij}^{S_1} := \frac{\omega_1|I|}{\Delta x+\Delta y}\max_q\left\{\frac{\left\|\nabla p^e(\mathbf{x}_{ij}^q)\right\|}{\rho^e(\mathbf{x}_{ij}^q)\sqrt{2e(\mathbf{x}_{ij}^q)}}\right\}, \qquad \widetilde{\alpha}_{ij}^{S_2} := \frac{\omega_1|I|}{\Delta x+\Delta y}\frac{\|\widetilde{\tau}\|}{\overline{\rho}_{ij}^e\sqrt{2\overline{e}_{ij}}}, \tag{4.30b}$$

where $|I| = \Delta x\Delta y$ and $\mathbf{x}_{ij}^q \in \mathbb{S}_{ij}$. Detailed proof of Theorem 3.2 is provided below.

Proof. We again decompose the proof into the following five steps:

Step 1: Decomposition. For an arbitrary parameter $\widetilde{\eta} \in (0, 1]$, the finite volume WENO method (2.13) can be rewritten as

$$\begin{aligned}\overline{\mathbf{U}}_{ij}^{n+1} &= \widetilde{\eta}\overline{\mathbf{U}}_{ij}^{n} - \lambda_1(\widehat{\mathbf{F}}_{i+\frac{1}{2},j} - \widehat{\mathbf{F}}_{i-\frac{1}{2},j}) - \lambda_2(\widehat{\mathbf{G}}_{i,j+\frac{1}{2}} - \widehat{\mathbf{G}}_{i,j-\frac{1}{2}}) + (1-\widetilde{\eta})\overline{\mathbf{U}}_{ij}^{n} + \Delta t\overline{\mathbf{S}}_{ij} \\ &= \left[\widetilde{\eta}\overline{\mathbf{U}}_{ij}^{n} - M_1 - M_2\right] + \left[M_1 + M_2 - \lambda_1(\widehat{\mathbf{F}}_{i+\frac{1}{2},j} - \widehat{\mathbf{F}}_{i-\frac{1}{2},j}) - \lambda_2(\widehat{\mathbf{G}}_{i,j+\frac{1}{2}} - \widehat{\mathbf{G}}_{i,j-\frac{1}{2}})\right] \\ &\quad + (1-\widetilde{\eta})\overline{\mathbf{U}}_{ij}^{n} + \Delta t\overline{\mathbf{S}}_{ij} =: \widetilde{\mathbf{W}}_1 + \widetilde{\mathbf{W}}_2 + \widetilde{\mathbf{W}}_3,\end{aligned}$$

where

$$M_1 = \frac{\lambda_1}{\lambda_1+\lambda_2}\omega_1\widetilde{\eta}\sum_{\nu=1}^{L}\omega_\nu\left(\mathbf{U}^{-}_{i+\frac{1}{2},\nu} + \mathbf{U}^{+}_{i-\frac{1}{2},\nu}\right),$$

$$M_2 = \frac{\lambda_2}{\lambda_1+\lambda_2}\omega_1\widetilde{\eta}\sum_{\nu=1}^{L}\omega_\nu\left(\mathbf{U}^{-}_{\nu,j+\frac{1}{2}} + \mathbf{U}^{+}_{\nu,j-\frac{1}{2}}\right).$$

Next we will prove that $\widetilde{\mathbf{W}}_1$, $\widetilde{\mathbf{W}}_2$ and $\widetilde{\mathbf{W}}_3$ are in the set G, and also select the suitable choice of the parameter $\widetilde{\eta}$ in Steps 2-5 below.

Step 2: $\widetilde{\mathbf{W}}_1 \in G$. For the term $\widetilde{\mathbf{W}}_1$, we consider the decomposition (4.28), which yields

$$\widetilde{\mathbf{W}}_1 := \widetilde{\eta}\overline{\mathbf{U}}_{ij}^{n} - M_1 - M_2 = \widetilde{\eta}\sum_{\nu_1=2}^{L-1}\sum_{\nu=1}^{L}\omega_\nu\omega_{\nu_1}\left(\frac{\lambda_2}{\lambda_1+\lambda_2}\mathbf{U}_{ij}(x_i^{\nu}, y_j^{\nu_1}) + \frac{\lambda_1}{\lambda_1+\lambda_2}\mathbf{U}_{ij}(x_i^{\nu_1}, y_j^{\nu})\right). \tag{4.31}$$

Therefore, we have $\widetilde{\mathbf{W}}_1 \in G$ following the assumption (3.21) and Lemma 2.1.

Step 3: $\widetilde{\mathbf{W}}_2 \in G$. The term $\widetilde{\mathbf{W}}_2$ can be further decomposed into two terms

$$\begin{aligned}\widetilde{\mathbf{W}}_2 =& \frac{\lambda_1}{\lambda_1+\lambda_2}\omega_1\widetilde{\eta}\sum_{\nu=1}^{L}\omega_\nu\left(\mathbf{U}^{-}_{i+\frac{1}{2},\nu} + \mathbf{U}^{+}_{i-\frac{1}{2},\nu}\right) - \lambda_1(\widehat{\mathbf{F}}_{i+\frac{1}{2},j} - \widehat{\mathbf{F}}_{i-\frac{1}{2},j}) \\ &+ \frac{\lambda_2}{\lambda_1+\lambda_2}\omega_1\widetilde{\eta}\sum_{\nu=1}^{L}\omega_\nu\left(\mathbf{U}^{-}_{\nu,j+\frac{1}{2}} + \mathbf{U}^{+}_{\nu,j-\frac{1}{2}}\right) - \lambda_2(\widehat{\mathbf{G}}_{i,j+\frac{1}{2}} - \widehat{\mathbf{G}}_{i,j-\frac{1}{2}}) \\ =:& \widetilde{\mathbf{W}}_{21} + \widetilde{\mathbf{W}}_{22}.\end{aligned}$$

The first term can be reformulated as follows:

$$\widetilde{\mathbf{W}}_{21} = \sum_{\nu=1}^{L}\widetilde{\eta}\omega_1\omega_\nu\frac{\lambda_1}{\lambda_1+\lambda_2}\mathbf{U}^{-}_{i+\frac{1}{2},\nu} - \lambda_1(\widehat{\mathbf{F}}_{i+\frac{1}{2},j} - \widehat{\mathbf{F}}^{*}_{ij}) + \sum_{\nu=1}^{L}\widetilde{\eta}\omega_1\omega_\nu\frac{\lambda_1}{\lambda_1+\lambda_2}\mathbf{U}^{+}_{i-\frac{1}{2},\nu} - \lambda_1(\widehat{\mathbf{F}}^{*}_{ij} - \widehat{\mathbf{F}}_{i-\frac{1}{2},j})$$

with the term $\widehat{\mathbf{F}}^{*}_{ij}$ defined by

$$\widehat{\mathbf{F}}^{*}_{ij} = \sum_{\nu}\omega_\nu\mathscr{F}^{hllc}\left(\frac{\rho^{e,+}_{i-\frac{1}{2},\nu}e^{\star,+}_{i-\frac{1}{2},\nu}}{(\rho e)^{e,+}_{i-\frac{1}{2},\nu}}\mathbf{U}^{+}_{i-\frac{1}{2},\nu}, \frac{\rho^{e,-}_{i+\frac{1}{2},\nu}e^{\star,-}_{i+\frac{1}{2},\nu}}{(\rho e)^{e,-}_{i+\frac{1}{2},\nu}}\mathbf{U}^{-}_{i+\frac{1}{2},\nu}\right) =: \sum_{\nu}\omega_\nu\mathscr{F}^{hllc,*}{}_{i\nu}. \tag{4.32}$$

With the WB numerical flux introduced in (4.24), we can further simplify this term as:

$$\widetilde{\mathbf{W}}_{21} = \widetilde{\eta}\frac{\lambda_1}{\lambda_1+\lambda_2}\omega_1\sum_{\nu=1}^{L}\omega_\nu\left(\frac{(\rho e)^{e,-}_{i+\frac{1}{2},\nu}}{\rho^{e,-}_{i+\frac{1}{2},\nu}e^{\star,-}_{i+\frac{1}{2},\nu}}\mathbf{W}^{+}_{21} + \frac{(\rho e)^{e,+}_{i-\frac{1}{2},\nu}}{\rho^{e,+}_{i-\frac{1}{2},\nu}e^{\star,+}_{i-\frac{1}{2},\nu}}\mathbf{W}^{-}_{21}\right),$$

where

$$\mathbf{W}^{+}_{21} = \frac{\rho^{e,-}_{i+\frac{1}{2},\nu}e^{\star,-}_{i+\frac{1}{2},\nu}}{(\rho e)^{e,-}_{i+\frac{1}{2},\nu}}\mathbf{U}^{-}_{i+\frac{1}{2},\nu} - \frac{\lambda_1+\lambda_2}{\widetilde{\eta}\omega_1}\frac{\rho^{e,-}_{i+\frac{1}{2},\nu}e^{\star,-}_{i+\frac{1}{2},\nu}}{(\rho e)^{e,-}_{i+\frac{1}{2},\nu}} \times (\mathscr{F}^{hllc}{}_{i+\frac{1}{2},j} - \mathscr{F}^{hllc,*}{}_{i\nu});$$

$$\mathbf{W}^{-}_{21} = \frac{\rho^{e,+}_{i-\frac{1}{2},\nu}e^{\star,+}_{i-\frac{1}{2},\nu}}{(\rho e)^{e,+}_{i-\frac{1}{2},\nu}}\mathbf{U}^{+}_{i-\frac{1}{2},\nu} - \frac{\lambda_1+\lambda_2}{\widetilde{\eta}\omega_1}\frac{\rho^{e,+}_{i-\frac{1}{2},\nu}e^{\star,+}_{i-\frac{1}{2},\nu}}{(\rho e)^{e,+}_{i-\frac{1}{2},\nu}} \times (\mathscr{F}^{hllc,*}{}_{i\nu} - \mathscr{F}^{hllc}{}_{i-\frac{1}{2},j}).$$

Similarly, the second term $\widetilde{\mathbf{W}}_{22}$ can be reformulated as follows:

$$\widetilde{\mathbf{W}}_{22} := \widetilde{\eta}\frac{\lambda_2}{\lambda_1+\lambda_2}\omega_1\sum_{\nu=1}^{L}\omega_\nu\left(\frac{(\rho e)^{e,-}_{\nu,j+\frac{1}{2}}}{\rho^{e,-}_{\nu,j+\frac{1}{2}}e^{\star,-}_{\nu,j+\frac{1}{2}}}\mathbf{W}^{+}_{22}+\frac{(\rho e)^{e,+}_{\nu,j-\frac{1}{2}}}{\rho^{e,+}_{\nu,j-\frac{1}{2}}e^{\star,+}_{\nu,j-\frac{1}{2}}}\mathbf{W}^{-}_{22}\right)$$

with

$$\mathbf{W}^{+}_{22}=\frac{\rho^{e,-}_{\nu,j+\frac{1}{2}}e^{\star,-}_{\nu,j+\frac{1}{2}}}{(\rho e)^{e,-}_{\nu,j+\frac{1}{2}}}\mathbf{U}^{-}_{\nu,j+\frac{1}{2}}-\frac{\lambda_1+\lambda_2}{\widetilde{\eta}\omega_1}\frac{\rho^{e,-}_{\nu,j+\frac{1}{2}}e^{\star,-}_{\nu,j+\frac{1}{2}}}{(\rho e)^{e,-}_{\nu,j+\frac{1}{2}}}\times(\mathscr{G}^{hllc}{}_{i,j+\frac{1}{2}}-\mathscr{G}^{hllc,*}{}_{\nu j}),$$

$$\mathbf{W}^{-}_{22}=\frac{\rho^{e,+}_{\nu,j-\frac{1}{2}}e^{\star,+}_{\nu,j-\frac{1}{2}}}{(\rho e)^{e,+}_{\nu,j-\frac{1}{2}}}\mathbf{U}^{+}_{\nu,j-\frac{1}{2}}-\frac{\lambda_1+\lambda_2}{\widetilde{\eta}\omega_1}\frac{\rho^{e,+}_{\nu,j-\frac{1}{2}}e^{\star,+}_{\nu,j-\frac{1}{2}}}{(\rho e)^{e,+}_{\nu,j-\frac{1}{2}}}\times(\mathscr{G}^{hllc,*}{}_{\nu j}-\mathscr{G}^{hllc}{}_{i,j-\frac{1}{2}}),$$

where the definitions of $\mathscr{G}^{hllc}{}_{i,j\pm\frac{1}{2}}$ and $\mathscr{G}^{hllc,*}{}_{\nu j}$ are similar to those for $\mathscr{F}^{hllc}{}_{i\pm\frac{1}{2},j}$ and $\mathscr{F}^{hllc,*}{}_{i\nu}$. In summary, according to Lemma 2.1 and Lemma 4.3, we have $\widetilde{\mathbf{W}}_{21}+\widetilde{\mathbf{W}}_{22}\in G$, under the condition $\Delta t\left(\frac{1}{\Delta x}+\frac{1}{\Delta y}\right)\widetilde{\alpha}^{F}_{ij}\le\widetilde{\eta}\omega_1$, with $\widetilde{\alpha}^{F}_{ij}$ defined in (4.30).

Step 4: $\widetilde{\mathbf{W}}_3\in G$. Now we consider the term $\widetilde{\mathbf{W}}_3$, and start by introducing an arbitrary parameter $\widetilde{\lambda}\in(0,1)$. Following the approach in [37], we have

$$\begin{aligned}\widetilde{\mathbf{W}}_3 &:= (1-\widetilde{\eta})\overline{\mathbf{U}}^{n}_{ij}+\Delta t\overline{\mathbf{S}}_{ij}=(1-\widetilde{\eta})\widetilde{\lambda}\sum_q\hat{\omega}_q\mathbf{U}(\mathbf{x}^q_{ij})+(1-\widetilde{\eta})(1-\widetilde{\lambda})\overline{\mathbf{U}}^{n}_{ij}+\Delta t\overline{\mathbf{S}}_{ij}\\ &=\sum_q\hat{\omega}_q\left[(1-\widetilde{\eta})\widetilde{\lambda}\mathbf{U}(\mathbf{x}^q_{ij})+\frac{\Delta t}{\rho^e(\mathbf{x}^q_{ij})}\begin{pmatrix}0\\ \rho(\mathbf{x}^q_{ij})\nabla p^e(\mathbf{x}^q_{ij})\\ \mathbf{m}(\mathbf{x}^q_{ij})\cdot\nabla p^e(\mathbf{x}^q_{ij})\end{pmatrix}\right]+\left[(1-\widetilde{\eta})(1-\widetilde{\lambda})\overline{\mathbf{U}}^{n}_{ij}+\frac{\Delta t}{\overline{\rho}^{e}_{ij}}\begin{pmatrix}0\\ \overline{\rho}_{ij}\widetilde{\tau}^{\top}\\ \overline{\mathbf{m}}_{ij}\cdot\widetilde{\tau}\end{pmatrix}\right].\end{aligned}$$

According to Lemma 2.2, we have $(1-\widetilde{\eta})\overline{\mathbf{U}}^{n}_{ij}+\Delta t\overline{\mathbf{S}}_{ij}\in G$, if

$$\Delta t\left(\frac{1}{\Delta x}+\frac{1}{\Delta y}\right)\widetilde{\alpha}^{S_1}_{ij}\le\omega_1(1-\widetilde{\eta})\widetilde{\lambda},\qquad\Delta t\left(\frac{1}{\Delta x}+\frac{1}{\Delta y}\right)\widetilde{\alpha}^{S_2}_{ij}\le\omega_1(1-\widetilde{\eta})(1-\widetilde{\lambda}).$$

Step 5: "optimal parameter". Similar to the 1D case, we take the following "optimal" parameters

$$\widetilde{\eta}^{*}=\frac{\widetilde{\alpha}^{F}_{ij}}{\widetilde{\alpha}_{ij}}\text{ and }\widetilde{\lambda}^{*}=\frac{\widetilde{\alpha}^{S_1}_{ij}}{\widetilde{\alpha}^{S_1}_{ij}+\widetilde{\alpha}^{S_2}_{ij}}\tag{4.33}$$

such that the $\overline{\mathbf{U}}^{n+1}_{ij}\in G$ under the CFL condition $\Delta t\left(\frac{1}{\Delta x}+\frac{1}{\Delta y}\right)\widetilde{\alpha}_{ij}\le\omega_1$. □

Remark 4.3. As discussed in Remark 4.2 for the 1D case, if both ϕ_x and ϕ_y are constants, the CFL-type condition (3.21) can be much simplified, which will be omitted here for saving space.

5. GLK-WB: Grosheintz-Laval and Käppeli's method

In this section, we will analyze the PP property of the WB WENO method developed by Grosheintz-Laval and Käppeli in [15] (abbreviated as "GLK-WB"). We will briefly review this method here, and refer to [15] for more details. The source term approximation is reformulated in an equivalent way so that the framework to prove the PP property in Section 4 can be easily applied.

In the GLK-WB method, the constant entropy is presented to fully characterize the equilibrium state. The relevant thermodynamic relation for isentropic hydrostatic equilibrium is

$$\mathrm{d}h=T\mathrm{d}s+\frac{\mathrm{d}p}{\rho},\tag{5.1}$$

where $h=e+p/\rho$ is the specific enthalpy and s is the specific entropy. The equilibrium state (2.1) for the isentropic case ($\mathrm{d}s=0$) can be rewritten as $\nabla h=\frac{1}{\rho}\nabla p=-\nabla\phi$, and integrating it yields

$$h+\phi=constant,\tag{5.2}$$

which is the targeting equilibrium state of the GLK-WB method in [15].

5.1. One-dimensional GLK-WB scheme

5.1.1. WB numerical flux and source term discretization

We start by reviewing the numerical flux and discretization of the source term in GLK-WB method in the 1D case. The standard LF numerical flux

$$\widehat{\mathbf{F}}_{j+\frac{1}{2}} = \mathscr{F}^{\mathrm{LF}}\left(\mathbf{U}^{-}_{j+\frac{1}{2}}, \mathbf{U}^{+}_{j+\frac{1}{2}}\right) = \frac{1}{2}\left[\mathbf{F}(\mathbf{U}^{-}_{j+\frac{1}{2}}) + \mathbf{F}(\mathbf{U}^{+}_{j+\frac{1}{2}}) - \alpha^{\mathrm{LF}}_{j+\frac{1}{2}}\left(\mathbf{U}^{+}_{j+\frac{1}{2}} - \mathbf{U}^{-}_{j+\frac{1}{2}}\right)\right], \tag{5.3}$$

is considered in [15], where $\alpha^{\mathrm{LF}}_{j+\frac{1}{2}} \geq \max\limits_{\mathbf{U}\in\{\mathbf{U}^{-}_{j+1/2}, \mathbf{U}^{+}_{j+1/2}\}} \alpha_{\max}(\mathbf{U})$ denotes the numerical viscosity parameter. In order to achieve the WB property, the GLK-WB method suggests building $\mathbf{U}^{\pm}_{j+\frac{1}{2}}$ via a fully equilibrium-preserving reconstruction

$$\mathbf{U}_j(x) = \mathbf{U}^{e}_j(x) + \delta\mathbf{U}_j(x). \tag{5.4}$$

Here $\mathbf{U}^{e}_j(x)$ and $\delta\mathbf{U}_j(x)$ are computed via the local hydrostatic reconstruction, which consists of the following two parts.

- First, we construct an equilibrium profile in each cell. Within the cell I_j, a subcell equilibrium reconstruction of the specific enthalpy

$$h^{e}_j(x) = h_{0,j} + \phi(x_j) - \phi(x), \tag{5.5}$$

is considered, with $h_{0,j}$ to be determined. Therefore, the equilibrium density $\rho^{e}_j(x)$ and internal energy density $(\rho e)^{e}_j(x)$ profiles can be computed, hence $\mathbf{U}^{e}_j(x)$. The constant $h_{0,j}$ and $s_{0,j}$ can be determined by solving

$$\overline{\rho}_j - \overline{\rho}^{e}_j = 0, \quad \textit{and} \quad \overline{\rho e}_j - \overline{(\rho e)}^{e}_j = 0, \tag{5.6}$$

where $\overline{\rho}_j$ and $\overline{\rho e}_j$ are the current numerical solutions and

$$\overline{\rho}^{e}_j := \mathscr{L}_j(\rho^{e}_j(x)), \qquad \overline{(\rho e)}^{e}_j := \mathscr{L}_j\left((\rho e)^{e}_j(x)\right). \tag{5.7}$$

Once $h_{0,j}$ and $s_{0,j}$ are fixed, we have the following high-order accurate representation of the equilibrium in the cell I_j:

$$\mathbf{U}^{e}_j(x) = \left(\rho^{e}_j(x), 0, (\rho e)^{e}_j(x)\right)^{\top}, \tag{5.8}$$

which can also be extended to neighboring cells to compute equilibrium perturbation cell averages $\overline{\mathbf{U}}_l - \mathscr{L}_l(\mathbf{U}^{e}_j(x))$, for $l = j,\ j\pm1, \cdots$.
- Second, the perturbation part $\delta\mathbf{U}_j(x)$ of the local hydrostatic reconstruction can be obtained by applying the high-order WENO-ZQ reconstruction procedure on the equilibrium perturbation cell averages:

$$\delta\mathbf{U}_j(x) = \mathscr{W}_j\left(\{\overline{\mathbf{U}}_l - \mathscr{L}_l(\mathbf{U}^{e}_j)\}\right) = \mathscr{W}_j\left(\{\overline{\delta\mathbf{U}}_l\}\right). \tag{5.9}$$

Remark 5.1. It is worth noting that in numerical simulations, $h^{e}_j(x)$ defined by (5.5) can be negative value at some points in the cell I_j. In this case, we should replace (5.5) with $h^{e}_j(x) = \max\{0, h_{0,j} + \phi(x_j) - \phi(x)\}$. The same treatment will also be employed in the 2D case.

The discretization of the source term integral is decomposed into two parts: the equilibrium part which can be directly integrated, and the perturbation part which is approximated by numerical quadrature. Specifically, the discretization of the source term integral in the momentum equation is computed by

$$\overline{S}^{[2]}_j = \frac{p^{e}_j(x_{j+\frac{1}{2}}) - p^{e}_j(x_{j-\frac{1}{2}})}{\Delta x} - \mathscr{L}_j\left(\delta\rho_j(x)\frac{\partial\phi}{\partial x}\right). \tag{5.10}$$

In fact, the above formula can also be rewritten as follows:

$$\begin{aligned}
\overline{S}^{[2]}_j &= \frac{p^{e}_j(x_{j+\frac{1}{2}}) - p^{e}_j(x_{j-\frac{1}{2}})}{\Delta x} + \mathscr{L}_j\left(\frac{\rho_j(x) - \rho^{e}_j(x)}{\rho^{e}_j(x)}(p^{e}_j)_x\right) \\
&= \frac{\overline{\rho}_j}{\overline{\rho}^{e}_j}\frac{\left(p^{e}_j(x_{j+\frac{1}{2}}) - p^{e}_j(x_{j-\frac{1}{2}})\right)}{\Delta x} + \mathscr{L}_j\left(\left(\frac{\rho_j(x)}{\rho^{e}_j(x)} - \frac{\overline{\rho}_j}{\overline{\rho}^{e}_j}\right)(p^{e}_j)_x\right) \\
&= \mathscr{L}_j\left(\frac{\rho_j(x)}{\rho^{e}_j(x)}(p^{e}_j)_x\right) + \frac{\overline{\rho}_j}{\overline{\rho}^{e}_j}\tau,
\end{aligned} \tag{5.11}$$

where the second equality uses the fact that $\overline{\rho}_j = \overline{\rho^e_j}$ in (5.6), and

$$\tau = \frac{1}{\Delta x}\left(p^e_j(x_{j+\frac{1}{2}}) - p^e_j(x_{j-\frac{1}{2}})\right) - \mathscr{L}_j\left((p^e_j)_x\right) \tag{5.12}$$

is the WB correction term for the 1D GLK-WB method. Note that this source term approximation takes a similar form as that in (4.4). In the original GLK-WB method [15], the source term integral $\overline{S}^{[3]}_j$ in the energy equation is approximated by a standard Gauss quadrature, which is sufficient for the WB property. However, we suggest, to accommodate the theoretical PP property, the following discretization should be adopted:

$$\overline{S}^{[3]}_j := \mathscr{L}_j\left(\frac{m_j(x)}{\rho^e_j(x)}(p^e_j)_x\right) + \frac{\overline{m}_j}{\overline{\rho^e_j}}\tau. \tag{5.13}$$

As an FV method (2.8) with the LF numerical flux (5.3) and source term discretization (5.10) and (5.13), the GLK-WB scheme can be shown to have the WB property, and preserves the discrete version of the hydrostatic equilibrium (5.2) (combined with $u = 0$) exactly. The proof can be found in [15] and is omitted here.

5.1.2. Analysis of PP property

First of all, we present the following lemma for LF numerical flux:

Lemma 5.1. *[50,51] For any constants $\lambda_M, \lambda \in \mathbb{R}^+$, and three admissible states $\mathbf{U}_L, \mathbf{U}_M, \mathbf{U}_R \in G$, we have*

$$\lambda_M \mathbf{U}_M - \lambda\left(\mathscr{F}^{\mathrm{LF}}(\mathbf{U}_M, \mathbf{U}_R) - \mathscr{F}^{\mathrm{LF}}(\mathbf{U}_L, \mathbf{U}_M)\right) \in G,$$

if $\lambda\alpha^{\mathrm{LF}} \le \lambda_M$.

Note that the equilibrium component $\mathbf{U}^e_j(x)$ may not necessarily be a polynomial vector, hence in general $\mathbf{U}_j(x)$ is not a polynomial vector. Nevertheless, the following identity still holds:

$$\underbrace{\mathscr{L}_j\left(\mathbf{U}^e_j(x) + \mathscr{W}_j(\{\delta\overline{\mathbf{U}}_l\})\right)}_{=\sum_{\nu=1}^{L}\omega_\nu \mathbf{U}_j(x^\nu_j)} = \mathscr{L}_j\left(\mathbf{U}^e_j(x)\right) + \delta\overline{\mathbf{U}}_j = \begin{pmatrix}\overline{\rho}_j\\ 0\\ \overline{\rho e}_j\end{pmatrix} + \begin{pmatrix}0\\ \overline{m}_j\\ \overline{E}_j - \overline{\rho e}_j\end{pmatrix} = \overline{\mathbf{U}}_j, \tag{5.14}$$

where (5.6), (5.7), (5.9) are used to derive the second equality, and we use the fact that $\mathscr{W}_j(\{\delta\overline{\mathbf{U}}_l\})$ is the WENO reconstructed polynomial whose cell average is same as $\delta\overline{\mathbf{U}}_j$ in the cell I_j.

We are now in the position to analyze the PP property of the GLK-WB scheme. Theorem 3.1 holds for the 1D GLK-WB scheme, with the parameter $\widetilde{\alpha}_j := \widetilde{\alpha}^F_j + \widetilde{\alpha}^{S_1}_j + \widetilde{\alpha}^{S_2}_j$ given by

$$\widetilde{\alpha}^F_j := \max_j\{\alpha^{\mathrm{LF}}_{j+\frac{1}{2}}\}, \quad \widetilde{\alpha}^{S_1}_j := \omega_1\Delta x \max_{1\le\nu\le L}\left\{\frac{\left|\left(p^e_j\right)_x(x^\nu_j)\right|}{\rho^e_j(x^\nu_j)\sqrt{2e(x^\nu_j)}}\right\}, \quad \widetilde{\alpha}^{S_2}_j := \omega_1\Delta x\frac{|\tau|}{\overline{\rho^e_j}\sqrt{2\overline{e}_j}}, \tag{5.15}$$

respectively, where $\widetilde{\alpha}^{S_1}_j + \widetilde{\alpha}^{S_2}_j = \mathscr{O}(\Delta x)$ for smooth $\rho^e(x)$ and $p^e(x)$.

Proof. Since the proof follows the same lines as that in Section 4.1.2, we shall only highlight the main steps and point out the differences.

Step 1: Decomposition. This same decomposition is introduced.

Step 2: $\mathbf{W}_1 \in G$. Note that (5.14) can be viewed as the analog of (4.15). Hence, from the assumption (3.19) and Lemma 2.1, we can easily conclude that $\mathbf{W}_1 \in G$.

Step 3: $\mathbf{W}_2 \in G$. In GLK-WB method, the LF numerical flux is used, and $\mathbf{W}_2$ can be decomposed into:

$$\begin{aligned}\mathbf{W}_2 = {}& \eta\omega_1\mathbf{U}^-_{j+\frac{1}{2}} - \frac{\Delta t}{\Delta x}\left[\mathscr{F}^{\mathrm{LF}}\left(\mathbf{U}^-_{j+\frac{1}{2}}, \mathbf{U}^+_{j+\frac{1}{2}}\right) - \mathscr{F}^{\mathrm{LF}}\left(\mathbf{U}^+_{j-\frac{1}{2}}, \mathbf{U}^-_{j+\frac{1}{2}}\right)\right]\\ & + \eta\omega_1\mathbf{U}^+_{j-\frac{1}{2}} - \frac{\Delta t}{\Delta x}\left[\mathscr{F}^{\mathrm{LF}}\left(\mathbf{U}^+_{j-\frac{1}{2}}, \mathbf{U}^-_{j+\frac{1}{2}}\right) - \mathscr{F}^{\mathrm{LF}}\left(\mathbf{U}^-_{j-\frac{1}{2}}, \mathbf{U}^+_{j-\frac{1}{2}}\right)\right].\end{aligned} \tag{5.16}$$

Thanks to Lemma 2.1, Lemma 5.1 and the assumption (3.19), we have $\mathbf{W}_2 \in G$ under the condition $\frac{\Delta t}{\Delta x}\widetilde{\alpha}^F_j \le \eta\omega_1$.

Step 4: $\mathbf{W}_3 \in G$. Since the source term approximations (5.10) and (5.13) are exactly the same as (4.4) and (4.6), we conclude

that $\mathbf{W}_3 \in G$ following the same analysis.

Step 5: "optimal" parameters. The "optimal" values of η and λ have the same form as in (4.21). Combining these results and using Lemma 2.1, we conclude that $\overline{\mathbf{U}}_j^{n+1} \in G$. □

5.2. Two-dimensional GLK-WB scheme

5.2.1. WB numerical flux and source term discretization

The 2D semidiscrete finite volume WENO method is given by (2.12). We consider the following LF numerical flux

$$\widehat{\mathbf{F}}_{i+\frac{1}{2},j} = \sum_{\nu} \omega_\nu \mathscr{F}^{\mathrm{LF}}\left(\mathbf{U}^-_{i+\frac{1}{2},\nu}, \mathbf{U}^+_{i+\frac{1}{2},\nu}\right) = \frac{1}{2}\sum_{\nu} \omega_\nu \left[\mathbf{F}(\mathbf{U}^-_{i+\frac{1}{2},\nu}) + \mathbf{F}(\mathbf{U}^+_{i+\frac{1}{2},\nu}) - \alpha^{\mathrm{LF}}_{i+\frac{1}{2},\nu}\left(\mathbf{U}^+_{i+\frac{1}{2},\nu} - \mathbf{U}^-_{i+\frac{1}{2},\nu}\right)\right], \tag{5.17}$$

$$\widehat{\mathbf{G}}_{i,j+\frac{1}{2}} = \sum_{\nu} \omega_\nu \mathscr{G}^{\mathrm{LF}}\left(\mathbf{U}^-_{\nu,j+\frac{1}{2}}, \mathbf{U}^+_{\nu,j+\frac{1}{2}}\right) = \frac{1}{2}\sum_{\nu} \omega_\nu \left[\mathbf{G}(\mathbf{U}^-_{\nu,j+\frac{1}{2}}) + \mathbf{G}(\mathbf{U}^+_{\nu,j+\frac{1}{2}}) - \alpha^{\mathrm{LF}}_{\nu,j+\frac{1}{2}}\left(\mathbf{U}^+_{\nu,j+\frac{1}{2}} - \mathbf{U}^-_{\nu,j+\frac{1}{2}}\right)\right], \tag{5.18}$$

where $\alpha^{\mathrm{LF}}_{i+\frac{1}{2},\nu} \geq \max\limits_{\mathbf{U}\in\{\mathbf{U}^-_{i+\frac{1}{2},\nu}, \mathbf{U}^+_{i+\frac{1}{2},\nu}\}} \alpha_{\max}(\mathbf{U})$ denotes the numerical viscosity parameter, and $\alpha^{\mathrm{LF}}_{\nu,j+\frac{1}{2}}$ is defined in a similar way.

The numerical flux is based on an equilibrium preserving reconstruction of $\mathbf{U}^{\pm}_{i+\frac{1}{2},\nu}$ defined by

$$\mathbf{U}_{ij}(\mathbf{x}) = \mathbf{U}^e_{ij}(\mathbf{x}) + \delta\mathbf{U}_{ij}(\mathbf{x}). \tag{5.19}$$

The flowchart of the local hydrostatic reconstruction is the same as the 1D case, with

$$\begin{aligned} \mathbf{U}^e_{ij}(\mathbf{x}) &= \left(\rho^e_{ij}(\mathbf{x}), \mathbf{0}, (\rho e)^e_{ij}(\mathbf{x})\right), \\ \delta\mathbf{U}_{ij}(\mathbf{x}) &= \mathscr{W}_{ij}(\{\overline{\mathbf{U}}_{g,l} - \mathscr{L}_{g,l}(\mathbf{U}^e_{ij})\}) =: \mathscr{W}_{ij}(\{\overline{\delta\mathbf{U}}_{g,l}\}). \end{aligned} \tag{5.20}$$

Based on the dimension-by-dimension approach, the source term discretization can be rewritten in the same way as in (5.11):

$$\overline{S}^{[2]}_{ij} = \mathscr{L}_{ij}\left(\frac{\rho_{ij}}{\rho^e_{ij}}(p^e_{ij})_x\right) + \frac{\overline{\rho}_{ij}}{\overline{\rho}^e_{ij}}\widetilde{\tau}_x, \tag{5.21a}$$

$$\overline{S}^{[3]}_{ij} = \mathscr{L}_{ij}\left(\frac{\rho_{ij}}{\rho^e_{ij}}(p^e_{ij})_y\right) + \frac{\overline{\rho}_{ij}}{\overline{\rho}^e_{ij}}\widetilde{\tau}_y, \tag{5.21b}$$

$$\overline{S}^{[4]}_{ij} = \mathscr{L}_{ij}\left(\frac{\mathbf{m}_{ij}}{\rho^e_{ij}}\cdot\nabla p^e_{ij}\right) + \frac{\overline{\mathbf{m}}_{ij}}{\overline{\rho}^e_{ij}}\cdot\widetilde{\tau}, \tag{5.21c}$$

with the WB correction term $\widetilde{\tau} = (\widetilde{\tau}_x, \widetilde{\tau}_y)$ given by

$$\begin{aligned} \widetilde{\tau}_x &= \frac{1}{\Delta x}\mathscr{L}_j\left(p^e_{ij}(x_{i+\frac{1}{2}}, y)\right) - \frac{1}{\Delta x}\mathscr{L}_j\left(p^e_{ij}(x_{i-\frac{1}{2}}, y)\right) - \mathscr{L}_{ij}\left((p^e_{ij})_x\right), \\ \widetilde{\tau}_y &= \frac{1}{\Delta y}\mathscr{L}_i\left(p^e_{ij}(x, y_{j+\frac{1}{2}})\right) - \frac{1}{\Delta y}\mathscr{L}_i\left(p^e_{ij}(x, y_{j-\frac{1}{2}})\right) - \mathscr{L}_{ij}\left((p^e_{ij})_y\right). \end{aligned} \tag{5.22}$$

With the LF numerical flux (5.17)-(5.18) and the source term discretization (5.21)-(5.22), the 2D GLK-WB scheme has the WB property, and its proof can be found in [15].

5.2.2. Analysis of PP property

Similar as the 1D case, the following formula on the decomposition of the cell average holds

$$\begin{aligned} &\underbrace{\frac{\lambda_1}{\lambda_1+\lambda_2}\mathscr{L}_{ij}\left(\mathbf{U}^e_{ij}(\mathbf{x}) + \mathscr{W}_{ij}(\{\overline{\delta\mathbf{U}}_{g,l}\})\right) + \frac{\lambda_2}{\lambda_1+\lambda_2}\mathscr{L}_{ij}\left(\mathbf{U}^e_{ij}(\mathbf{x}) + \mathscr{W}_{ij}(\{\overline{\delta\mathbf{U}}_{g,l}\}\right)}_{\mathbf{LHS}} \\ &= \frac{\lambda_1}{\lambda_1+\lambda_2}\left(\mathscr{L}_{ij}\left(\mathbf{U}^e_{ij}(\mathbf{x})\right) + \overline{\delta\mathbf{U}}_{ij}\right) + \frac{\lambda_2}{\lambda_1+\lambda_2}\left(\mathscr{L}_{ij}\left(\mathbf{U}^e_{ij}(\mathbf{x})\right) + \overline{\delta\mathbf{U}}_{ij}\right) \\ &= \begin{pmatrix} \overline{\rho}_{ij} \\ \mathbf{0} \\ \overline{\rho e}_{ij} \end{pmatrix} + \begin{pmatrix} 0 \\ \overline{\mathbf{m}}_{ij} \\ \overline{E}_{ij} - \overline{\rho e}_{ij} \end{pmatrix} = \overline{\mathbf{U}}_{ij}, \end{aligned} \tag{5.23}$$

where **LHS** can be expanded as

$$\mathbf{LHS} = \sum_{\nu=1}^{L} \omega_1\omega_\nu \left(\frac{\lambda_2}{\lambda_1+\lambda_2} \left(\mathbf{U}_{ij}\left(x_i^\nu, y_{j-\frac{1}{2}}\right) + \mathbf{U}_{ij}\left(x_i^\nu, y_{j+\frac{1}{2}}\right)\right) + \frac{\lambda_1}{\lambda_1+\lambda_2} \left(\mathbf{U}_{ij}\left(x_{i-\frac{1}{2}}, y_j^\nu\right) + \mathbf{U}_{ij}\left(x_{i+\frac{1}{2}}, y_j^\nu\right)\right)\right) + \sum_{\nu_1=2}^{L-1}\sum_{\nu=1}^{L} \omega_\nu\omega_{\nu_1} \left(\frac{\lambda_2}{\lambda_1+\lambda_2}\mathbf{U}_{ij}\left(x_i^\nu, y_j^{\nu_1}\right) + \frac{\lambda_1}{\lambda_1+\lambda_2}\mathbf{U}_{ij}\left(x_i^{\nu_1}, y_j^\nu\right)\right). \tag{5.24}$$

The PP property of the 2D GLK-WB scheme can be found in Theorem 3.2, with the parameter $\widetilde{\alpha}_{ij} := \widetilde{\alpha}_{ij}^F + \widetilde{\alpha}_{ij}^{S_1} + \widetilde{\alpha}_{ij}^{S_2}$ given by

$$\widetilde{\alpha}_{ij}^F := \max_{i,j,\nu} \left\{ \alpha^{\mathrm{LF}}_{i+\frac{1}{2},\nu}, \alpha^{\mathrm{LF}}_{\nu,j+\frac{1}{2}} \right\}, \tag{5.25a}$$

$$\widetilde{\alpha}_{ij}^{S_1} := \frac{\omega_1|I|}{\Delta x+\Delta y} \max_q \left\{ \frac{1}{\rho_{ij}^e(\mathbf{x}_{ij}^q)} \frac{\left\|\nabla p_{ij}^e(\mathbf{x}_{ij}^q)\right\|}{\sqrt{2e(\mathbf{x}_{ij}^q)}} \right\}, \tag{5.25b}$$

$$\widetilde{\alpha}_{ij}^{S_2} := \frac{\omega_1|I|}{\Delta x+\Delta y} \frac{\|\widetilde{\tau}\|}{\overline{\rho}_{ij}^e\sqrt{2\overline{e}_{ij}}}. \tag{5.25c}$$

Proof. Since the proof follows the same lines as that in Section 4.2.2, we shall only highlight the main steps and point out the differences.

Step 1: Decomposition. This same decomposition is introduced.

Step 2: $\widetilde{\mathbf{W}}_1 \in G$. Note that (5.23) can be viewed as the analog of (4.28). Hence, from the assumption (3.21) and Lemma 2.1, we can conclude that $\widetilde{\mathbf{W}}_1 \in G$.

Step 3: $\widetilde{\mathbf{W}}_2 \in G$. Similar to the analysis of $\mathbf{W}_2 \in G$ in the 1D case as in (5.16), it is easy to show that $\widetilde{\mathbf{W}}_2 \in G$ under the condition $\Delta t\left(\frac{1}{\Delta x}+\frac{1}{\Delta y}\right)\widetilde{\alpha}_{ij}^F \le \widetilde{\eta}\omega_1$.

Step 4: $\widetilde{\mathbf{W}}_3 \in G$. Because the source term approximation (5.21) is exactly the same as (4.26) (with the only difference being the definition of $\mathbf{U}^e$), the analysis of $\widetilde{\mathbf{W}}_3 \in G$ is the same as its analogue in Section 4.2.2.

Step 5: "optimal" parameters. The "optimal" values of $\widetilde{\eta}$ and $\widetilde{\lambda}$ have the same form as in (4.33), and we obtain $\overline{\mathbf{U}}_{ij}^{n+1} \in G$ under the CFL condition (3.22). □

6. KPS-WB: Klingenberg, Puppo, and Semplice's method

In this section, we will analyze the PP property of the third WB WENO method, recently developed by Klingenberg, Puppo, and Semplice in [20] (abbreviated as "KPS-WB" scheme). We will briefly review the KPS-WB method and refer to [20] for more details. We only focus on the ideal gas in this section.

6.1. One-dimensional KPS-WB scheme

6.1.1. WB numerical flux and source term discretization

Consider hydrostatic stationary solutions $\rho^e(x)$ and $p^e(x)$, satisfying $\nabla p^e = -\rho^e\nabla\phi$, which is the targeting equilibrium state. The LF numerical flux (5.3) is used in the KPS-WB method, in which the numerical viscosity parameter satisfying $\alpha^{\mathrm{LF}}_{j+\frac{1}{2}} \ge \max_{\mathbf{U}\in\{\mathbf{U}^-_{j+\frac{1}{2}},\mathbf{U}^+_{j+\frac{1}{2}}\}} \alpha^{id}_{\max}(\mathbf{U})$ with $\alpha^{id} = |u| + \sqrt{\gamma\frac{p}{\rho}}$, where the superscript "id" indicates the ideal gas. In fact, any numerical flux can be used, which has been commented in [20, Remark 1].

In order to achieve the WB property, the KPS-WB method suggests to reconstruct the fluctuations of $\rho(x,t)$ and $p(x,t)$ from ρ^e and p^e. Denote them by $r(x)$ and $\pi(x)$, i.e.,

$$\rho(x) = \rho^e(x) + r(x), \quad p(x) = p^e(x) + \pi(x). \tag{6.1}$$

To do so, we first compute cell average values of auxiliary variables $r(x)$

$$\overline{r}_j = \overline{\rho}_j - \mathscr{R}_j\left(\rho^e(x)\right) = \overline{\rho}_j - \overline{\rho}_j^e, \tag{6.2}$$

and then apply the WENO reconstruction operator to obtain $r_j(x)$ via $\mathscr{W}_j(\{\overline{r}_l\})$, hence $\rho_j(x) = \mathscr{W}_j(\{\overline{r}_l\}) + \rho^e(x)$. The momentum polynomial $m_j(x)$ can be obtained via $\mathscr{W}_j(\{\overline{m}_l\})$. To recover the total energy, we first compute cell average values of auxiliary variables $\pi(x)$ as

$$\overline{\pi}_j = \overline{p}_j - \mathscr{R}_j\left(p^e(x)\right) = \overline{p}_j - \overline{p}^e_j, \tag{6.3}$$

where $\overline{p}_j = (\gamma-1)\left(\overline{E}_j - \overline{E_k}_j\right)$ with $\overline{E_k}_j = \mathscr{R}_j\left(m_j(x)^2/2/\rho_j(x)\right)$ using the WENO reconstructed $m(x)$ and $\rho(x)$ from above. Then the pressure can be recovered as $p_j(x) = \mathscr{W}_j(\{\overline{\pi}_l\}) + p^e(x)$. Therefore, the conservative variables can be recovered as follows:

$$\mathbf{U}_j(x) = \begin{pmatrix} \rho_j(x) \\ m_j(x) \\ \frac{p_j(x)}{\gamma-1} + \frac{(m_j(x))^2}{2\rho_j(x)} \end{pmatrix} = \begin{pmatrix} \mathscr{W}_j(\{\overline{r}_l\}) + \rho^e(x) \\ \mathscr{W}_j(\{\overline{m}_l\}) \\ \frac{\mathscr{W}_j(\{\overline{\pi}_l\})+p^e(x)}{\gamma-1} + \frac{1}{2}\frac{(\mathscr{W}_j(\{\overline{m}_l\}))^2}{\mathscr{W}_j(\{\overline{r}_l\})+\rho^e(x)} \end{pmatrix}, \tag{6.4}$$

which can be used to evaluate the values at the interfaces and interior Romberg's quadrature nodes.

Next, we consider the WB source term discretization of momentum and energy equations

$$\overline{S}^{[2]}_j \approx \frac{1}{\Delta x}\int_{x_{j-\frac{1}{2}}}^{x_{j+\frac{1}{2}}} \frac{\rho}{\rho^e} p^e_x dx \quad \text{and} \quad \overline{S}^{[3]}_j \approx \frac{1}{\Delta x}\int_{x_{j-\frac{1}{2}}}^{x_{j+\frac{1}{2}}} \frac{m}{\rho^e} p^e_x dx. \tag{6.5}$$

Romberg's method [20] is used to achieve the high-order WB approximation. Let us decompose the cell I_j into 2^l ($l \geq \frac{k-1}{2}, l \in \mathbb{N}^*$) equal subintervals of size $\Delta x/2^l$, and the nodes are denoted by $x^\kappa_j = x_{j-\frac{1}{2}} + \frac{(\kappa-1)}{2^l}\Delta x,\ \kappa = 1, \cdots, 2^l+1 = N$. We first introduce the following second-order WB form as the basis of the WB source term approximation: for a function $w = \rho$ or m,

$$Q^{(0)}_{2^l}(w) = \frac{1}{2}\sum_{\kappa=1}^{2^l}\left(\frac{w(x^\kappa_j)}{\rho^e(x^\kappa_j)} + \frac{w(x^{\kappa+1}_j)}{\rho^e(x^{\kappa+1}_j)}\right)\frac{p^e(x^{\kappa+1}_j) - p^e(x^\kappa_j)}{\Delta x} \quad for\ \ l \geq 0.$$

When $l = 0$, $Q^{(0)}_1$ is a second order WB approximation of source term [20]. To obtain a higher-order approximation without losing the WB property, Romberg's method is applied, which requires us to define the following recursion

$$Q^{(n)}_{2^l}(w) = \frac{4^n Q^{(n-1)}_{2^l}(w) - Q^{(n-1)}_{2^{l-1}}(w)}{4^n - 1} \qquad for\ \ l \geq 1, \quad n = 1, 2, \cdots, l. \tag{6.6}$$

For example, for the example $l = 2$, we have the following equality from (6.6)

$$Q^{(2)}_4(w) = \frac{16}{15}Q^{(1)}_4(w) - \frac{1}{15}Q^{(1)}_2(w) = \frac{16}{15}\left(\frac{4}{3}Q^0_4(w) - \frac{1}{3}Q^{(0)}_2(w)\right) - \frac{1}{15}\left(\frac{4}{3}Q^0_2(w) - \frac{1}{3}Q^{(0)}_1(w)\right).$$

The WB source term discretization in the momentum equation and energy equation with $(k+1)$th order accuracy can be written and simplified as

$$S^{[2]}_j = Q^{(l)}_{2^l}(\rho) = \sum_{\kappa=1}^{N}\omega_\kappa \frac{\rho(x^\kappa_j)}{\rho^e(x^\kappa_j)}A^\kappa_j, \quad S^{[3]}_j = Q^{(l)}_{2^l}(m) = \sum_{\kappa=1}^{N}\omega_\kappa \frac{m(x^\kappa_j)}{\rho^e(x^\kappa_j)}A^\kappa_j. \tag{6.7}$$

where the term A_j is a vector depending on average values of p^e_x in the subcells of I_j, and the specific forms of A_j for $k = 1, 3, 5$ are presented in Appendix A.

The 1D `KPS-WB` method (2.8) with LF numerical flux (5.3) and the source term approximation (6.7) has the WB property, and we refer to [20] for the proof.

6.1.2. Analysis of PP property

Theorem 3.1 on the PP property holds for the `KPS-WB` scheme, with the parameter $\widetilde{\alpha}_j := \widetilde{\alpha}^F_j + \widetilde{\alpha}^{S_1}_j$ defined by

$$\widetilde{\alpha}^F_j := \max_j\{\alpha^{\mathrm{LF}}_{j+\frac{1}{2}}\}, \quad \widetilde{\alpha}^{S_1}_j := \omega_1\Delta x \max_{1\leq\kappa\leq N}\left\{\frac{\left|A^\kappa_j\right|}{\rho^e(x^\kappa_j)\sqrt{2e(x^\kappa_j)}}\right\}, \tag{6.8}$$

where A^κ_j depends on average values of p^e_x in the subcells of I_j.

Proof. Since the proof follows the same lines as that in Section 4.1.2, we shall only highlight the main steps and point out the differences.

Step 1: Decomposition. This same decomposition is introduced.

Step 2: $\mathbf{W}_1 \in G$. Similar to the equality (4.15), the following identity holds for the `KPS-WB` method

$$\mathscr{R}_j(\mathbf{U}_j(x)) = \begin{pmatrix} \mathscr{R}_j(\mathscr{W}_j(\{\overline{r}_l\}) + \rho^e(x)) \\ \mathscr{R}_j(\mathscr{W}_j(\{\overline{m}_l\})) \\ \mathscr{R}_j(\frac{\mathscr{W}_j(\{\overline{\pi}_l\}) + p^e(x)}{\gamma - 1}) + \overline{E}_{kj}, \end{pmatrix} = \begin{pmatrix} \overline{r}_j + \overline{\rho}^e_j \\ \overline{m}_j \\ \overline{E}_j - \overline{E}_{kj} + \overline{E}_{kj} \end{pmatrix} = \begin{pmatrix} \overline{\rho}_j \\ \overline{m}_j \\ \overline{E}_j \end{pmatrix} = \overline{\mathbf{U}}_j.$$

Hence $\mathbf{W}_1 \in G$, according to Lemma 2.1 and the assumption (3.19).

Step 3: $\mathbf{W}_2 \in G$. Following the proof of $\mathbf{W}_2 \in G$ in Step 3 in Section 5.1.2, we have $\mathbf{W}_2 \in G$ if $\frac{\Delta t}{\Delta x}\widetilde{\alpha}^F_j \le \eta\omega_1$ with ω_1 being the quadrature weight in the Romberg's quadrature rule.

Step 4: $\mathbf{W}_3 \in G$. We can rewrite the vector $\mathbf{W}_3$ in the KPS-WB method as

$$(1-\eta)\overline{\mathbf{U}}^n_j + \Delta t\overline{\mathbf{S}}_j = \sum_{\kappa=1}^{N} \omega_\kappa \left[(1-\eta)\mathbf{U}_j(x^\kappa_j) + \Delta t \frac{A^\kappa_j}{\rho^e_j(x^\kappa_j)} \big(0, \rho_j(x^\kappa_j), m_j(x^\kappa_j)\big)^\top \right],$$

where A^κ_j depends on average values of p^e_x in the subcells of I_j. Thanks to Lemma 2.2, we have $\mathbf{W}_3 \in G$ for all κ, if $\frac{\Delta t}{\Delta x}\widetilde{\alpha}^{S_1}_j \le \omega_1(1-\eta)$.

Step 5: "optimal" parameters. We specify η to be the "optimal" parameter $\eta^* = \frac{\widetilde{\alpha}^F_j}{\widetilde{\alpha}_j}$. Combining these results and using Lemma 2.1, we conclude that $\overline{\mathbf{U}}^{n+1}_j \in G$. □

6.2. Two-dimensional KPS-WB scheme

6.2.1. WB numerical flux and source term discretization

The 2D semidiscrete finite volume WENO method takes the form (2.12), with the LF numerical flux (5.17)-(5.18). The reconstruction of $\mathbf{U}^{\pm}_{i+\frac{1}{2},\nu}$ is similar to the 1D case, with the introduction of variables

$$r(\mathbf{x}) = \rho(\mathbf{x}) - \rho^e(\mathbf{x}), \quad \pi(\mathbf{x}) = p(\mathbf{x}) - p^e(\mathbf{x}). \tag{6.9}$$

We skip the details and refer interested readers to [20].

For the discretization of the 2D source term in [20], Romberg's quadrature is used in one direction and the Gauss quadrature is used in the other direction. However, in this paper, Romberg's quadrature will be used in both directions at the same time. One purpose of doing this is to reduce the number of Gaussian quadrature points, and the other purpose is to simplify the analysis of the PP property. The discretization of source terms takes the form

$$S^{[2]}_{ij} = \sum_q \hat{\omega}_q \frac{\rho(\mathbf{x}^q_{ij})}{\rho^e(\mathbf{x}^q_{ij})} \tau^x(\mathbf{x}^q_{ij}), \qquad S^{[3]}_{ij} = \sum_q \hat{\omega}_q \frac{\rho(\mathbf{x}^q_{ij})}{\rho^e(\mathbf{x}^q_{ij})} \tau^y(\mathbf{x}^q_{ij}), \tag{6.10a}$$

$$S^{[4]}_{ij} = \sum_q \hat{\omega}_q \frac{m(\mathbf{x}^q_{ij})}{\rho^e(\mathbf{x}^q_{ij})} \tau^x(\mathbf{x}^q_{ij}) + \sum_q \hat{\omega}_q \frac{n(\mathbf{x}^q_{ij})}{\rho^e(\mathbf{x}^q_{ij})} \tau^y(\mathbf{x}^q_{ij}), \tag{6.10b}$$

where both τ^x and τ^y are $N \times N$ matrices ($N = 2^{\frac{k-1}{2}} + 1$) presented in Appendix A. Such 2D KPS-WB scheme has the WB property, and the proof can be found in [20].

6.2.2. Analysis of PP property

The PP property of the 2D KPS-WB scheme can be found in Theorem 3.2, with the parameter $\widetilde{\alpha}_{ij} := \widetilde{\alpha}^F_{ij} + \widetilde{\alpha}^{S_1}_{ij} + \widetilde{\alpha}^{S_2}_{ij}$ given by

$$\widetilde{\alpha}^F_{ij} := \max_{i,j,\kappa} \left\{ \alpha^{\mathrm{LF}}_{i+\frac{1}{2},\kappa}, \alpha^{\mathrm{LF}}_{\kappa,j+\frac{1}{2}} \right\}, \tag{6.11a}$$

$$\widetilde{\alpha}^{S_1}_{ij} := \left(\frac{\omega_1 |I|}{\Delta x + \Delta y} \right) \max_{\kappa,\nu} \left\{ \frac{1}{\rho^e(\mathbf{x}^q_{ij})} \frac{\|\mathbf{a}\|}{\sqrt{2e(\mathbf{x}^q_{ij})}} \right\}, \tag{6.11b}$$

$$\widetilde{\alpha}^{S_2}_{ij} := \left(\frac{\omega_1 |I|}{\Delta x + \Delta y} \right) \max_{\kappa,\nu} \left\{ \frac{1}{\rho^e(\mathbf{x}^q_{ij})} \frac{\|\mathbf{b}\|}{\sqrt{2e(\mathbf{x}^q_{ij})}} \right\}, \tag{6.11c}$$

where $\mathbf{a} = (\tau^x, \mathbf{0})$ and $\mathbf{b} = (\mathbf{0}, \tau^y)$.

Proof. Since the proof follows the same lines as that in Section 4.2.2, we shall only highlight the main steps and point out the differences.

Step 1: Decomposition. This same decomposition is introduced.

Step 2: $\widetilde{\mathbf{W}}_1 \in G$. Similar to the 1D case, we can obtain $\widetilde{\mathbf{W}}_1 \in G$ following (3.21) and Lemma 2.1.

Step 3: $\widetilde{\mathbf{W}}_2 \in G$. Similar to the analysis of $\mathbf{W}_2 \in G$ in the 1D case in (5.16), it is easy to show that $\widetilde{\mathbf{W}}_2 \in G$ under the condition $\Delta t \left(\frac{1}{\Delta x} + \frac{1}{\Delta y}\right) \widetilde{\alpha}_{ij}^F \le \widetilde{\eta}\omega_1$.

Step 4: $\widetilde{\mathbf{W}}_3 \in G$. For the `KPS-WB` method, the term $\widetilde{\mathbf{W}}_3$ can be decomposed into

$$\begin{aligned}
\widetilde{\mathbf{W}}_3 &= (1-\widetilde{\eta})\left(\widetilde{\lambda}\sum_q \hat{\omega}_q \mathbf{U}(\mathbf{x}_{ij}^q) + (1-\widetilde{\lambda})\sum_q \hat{\omega}_q \mathbf{U}(\mathbf{x}_{ij}^q)\right) + \Delta t \overline{\mathbf{S}}_{ij} \\
&= \sum_q \hat{\omega}_q \left[(1-\widetilde{\eta})\widetilde{\lambda}\mathbf{U}(\mathbf{x}_{ij}^q) + \frac{\Delta t}{\rho^e(\mathbf{x}_{ij}^q)}\begin{pmatrix} 0 \\ \rho(\mathbf{x}_{ij}^q)\mathbf{a}_q \\ \mathbf{m}(\mathbf{x}_{ij}^q)\cdot\mathbf{a}_q \end{pmatrix}\right] \\
&\quad + \sum_q \hat{\omega}_q \left[(1-\widetilde{\eta})(1-\widetilde{\lambda})\mathbf{U}(\mathbf{x}_{ij}^q) + \frac{\Delta t}{\rho^e(\mathbf{x}_{ij}^q)}\begin{pmatrix} 0 \\ \rho(\mathbf{x}_{ij}^q)\mathbf{b}_q \\ \mathbf{m}(\mathbf{x}_{ij}^q)\cdot\mathbf{b}_q \end{pmatrix}\right].
\end{aligned}$$

According to Lemma 2.2, we conclude that $\widetilde{\mathbf{W}}_3 \in G$, if

$$\Delta t \left(\frac{1}{\Delta x} + \frac{1}{\Delta y}\right) \widetilde{\alpha}_{ij}^{S_1} \le \omega_1 (1-\widetilde{\eta})\widetilde{\lambda} \quad \text{and} \quad \Delta t \left(\frac{1}{\Delta x} + \frac{1}{\Delta y}\right) \widetilde{\alpha}_{ij}^{S_2} \le \omega_1 (1-\widetilde{\eta})(1-\widetilde{\lambda}).$$

Step 5: "optimal" parameters. The "optimal" values of $\widetilde{\eta}$ and $\widetilde{\lambda}$ have the same form as in (4.33), we obtain $\overline{\mathbf{U}}_{ij}^{n+1} \in G$ under the CFL condition $\Delta t \left(\frac{1}{\Delta x} + \frac{1}{\Delta y}\right) \widetilde{\alpha}_{ij} \le \omega_1$. □

7. Numerical examples

In this section, we present extensive 1D and 2D numerical examples to validate the WB and PP properties of the proposed methods. For comparison, we will also present numerical results of non-well-balanced ("non-WB") FV WENO schemes with the standard HLLC flux. We use the explicit third-order SSP-RK time discretization and the ideal gas with $\gamma = 1.4$ in (1.3), unless otherwise stated. The CFL number is taken as 0.4 as discussed in Remark 3.1. In the 1D and 2D accuracy tests only, we use $\Delta t = 0.4\Delta x^{\frac{5}{3}}/\widetilde{\alpha}$ for the fifth-order scheme in order to match the temporal and spatial accuracy. The linear weights in the WENO-ZQ reconstruction (2.17) are taken $\gamma_1 = 0.998$ and $\gamma_2 = \gamma_3 = 0.001$. In all the numerical examples, the cell averages of the initial solution at $t = 0$ are computed via the fifth order Gauss-Lobatto quadrature. We also compute the cell averages of ρ^e and p^e in a similar way.

Example 1 (Accuracy test). This example is used to test the high-order accuracy of WENO schemes. Consider the exact solutions given by

$$\rho(x,t) = 1 + \frac{1}{5}sin(\pi(x-u_0t)), \qquad u(x,t) = 1, \qquad p(x,t) = \frac{9}{2} - (x-u_0t) + \frac{1}{5\pi}cos(\pi(x-u_0t)),$$

with the static gravitational field $\phi(x) = gx = x$ on the computational domain $x \in [0,2]$. We perform the simulation up to $T = 0.1$, and use the exact solutions on the ghost cells for the boundary treatment. All three WB PP methods have been tested, and Table 7.1 lists their numerical errors and convergence rates at different grid resolutions. It can be observed that the fifth-order convergence is achieved for all three methods, and the modified HLLC flux does not affect the accuracy of the `New-WB` method.

Example 2. (1D polytropic equilibrium). We use this example to test the well-balancedness of three methods for the polytropic equilibrium states. The stationary hydrostatic solutions are given by

$$\rho^e(x) = \left(\rho_0^{\gamma-1} - \frac{1}{K_0}\frac{\gamma-1}{\gamma}gx\right)^{\frac{1}{\gamma-1}}, \qquad u^e(x) = 0, \qquad p^e(x) = K_0(\rho^e(x))^\gamma, \tag{7.1}$$

where $g = 1, \gamma = \frac{5}{3}$, $\rho_0 = p_0 = 1$, and $K_0 = p_0/\rho_0^\gamma$. The gravitational potential $\phi(x) = gx$ on the computational domain $x \in [0,2]$. Both bounds are arranged as outflow boundary conditions.

To validate the well-balancedness of the three methods, we use double precision to perform the computation with the initial data (7.1), and simulate this problem up to $T = 4$. Table 7.2 lists L_1 errors of numerical solutions, which shows that

Table 7.1
Example 1. L_1 errors and convergence rates of three methods.

New-WB							
N	ρ		m		E	
32	1.94e-07	–	2.12e-07	–	2.51e-07	–
64	6.13e-09	4.98	6.63e-09	5.00	7.90e-09	4.99
128	1.92e-10	4.99	2.06e-10	5.00	2.47e-10	4.99
256	6.02e-12	4.99	6.46e-12	5.00	7.87e-12	4.97
GLK-WB						
N	ρ		m		E	
32	7.28e-07	–	7.30e-07	–	4.88e-07	–
64	2.53e-08	4.84	2.57e-08	4.82	2.38e-08	4.35
128	7.19e-10	5.13	7.18e-10	5.16	5.20e-10	5.51
256	2.25e-11	4.99	2.24e-11	5.00	1.46e-11	5.15
KPS-WB						
N	ρ		m		E	
32	7.27e-07	–	7.30e-07		4.80e-07	–
64	2.29e-08	4.98	2.29e-08	4.99	1.49e-08	5.00
128	7.19e-10	4.99	7.17e-10	4.99	4.68e-10	5.00
256	2.24e-11	4.99	2.24e-11	4.99	1.47e-11	4.98

Table 7.2
Example 2. L_1 errors of three methods with equilibrium initial data.

	New-WB			GLK-WB			KPS-WB		
N	ρ	m	E	ρ	m	E	ρ	m	E
100	1.00e-14	1.21e-15	3.21e-14	9.40e-15	4.95e-16	2.93e-14	7.21e-15	7.35e-16	2.35e-14
200	2.07e-14	2.32e-15	6.83e-14	2.04e-14	8.9e-16	6.30e-14	1.55e-14	1.30e-15	4.90e-14

Table 7.3
Example 2. L_1 errors of non-WB method with equilibrium initial data.

N	ρ		m		E	
50	2.45e-08	–	2.66e-08	–	2.57e-08	–
100	7.21e-10	5.08	7.50e-10	5.14	7.29e-10	5.14
200	1.91e-11	5.23	1.91e-11	5.29	1.86e-11	5.29

the numerical errors are all at the level of round-off error, therefore these methods have well-balanced properties. For comparison, we also listed L_1 errors of the non-WB scheme in Table 7.3, and observe that the errors did not reduce to the expected round-off error, although the fifth-order accuracy is obtained.

Next, in order to compare the performance of WB and non-WB schemes in capturing the small perturbation of equilibrium states, we add a small periodic velocity perturbation

$$u(0,t) = A\sin(4\pi t)$$

with $A = 10^{-9}$ at the left boundary. The solutions are computed up to $T = 1.5$. The pressure perturbation and the velocity computed by three WB methods and non-WB methods on 100 cells are plotted in the top row of Fig. 7.1, in which the reference solutions are computed using 500 computational cells. It can be observed the three methods perform very well in capturing the small perturbation of equilibrium states, while the non-WB method performs poorly, especially in the region where $x > 1.5$.

In the last test case, we consider the perturbation with a larger amplitude $A = 10^{-1}$. We perform the simulation until $T = 1.5$, the pressure perturbation and the velocity computed by the proposed methods and non-WB method on a mesh of 200 cells are plotted in the middle row of Fig. 7.1, together with a reference solution computed on 1000 cells. Both WB and non-WB methods can produce satisfactory results, which shows that the performance of the two types of methods is similar in capturing solutions that are far away from steady states. Finally, we adopt the New-WB method with (unmodified) traditional WENO-ZQ reconstruction for the case of $A = 10^{-1}$, as shown in the bottom row of Fig. 7.1. Some oscillations and overfitting phenomena near the shock wave can be observed, which may be due to the lack of scaling-invariant property as discussed in Remark 2.1.

Example 3 (Test on the PP property). We consider a gravitational field $\phi(x) = x^2/2$ centered around $x = 0$. The initial state is given by [50]

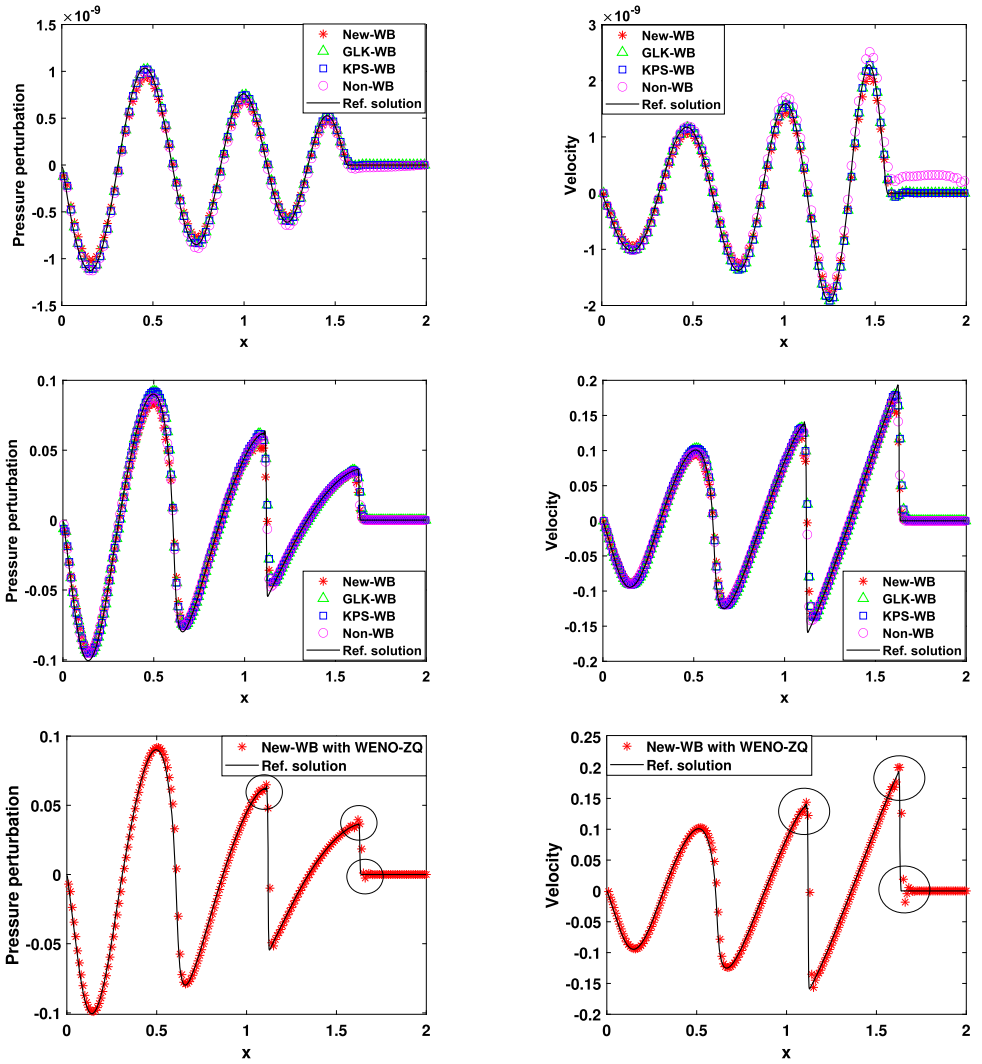

Fig. 7.1. Example 2, Top-Row: the propagation of small perturbation with $A = 10^{-9}$ by various methods in the polytropic hydrostatic atmosphere. Middle-Row: the propagation of small perturbation with $A = 10^{-1}$ by various methods in the polytropic hydrostatic atmosphere. Bottom-Row: Small perturbation with $A = 10^{-1}$ by the `New-WB` method with (unmodified) classical WENO-ZQ reconstruction. Left: Pressure perturbation; Right: Velocity.

$$\rho(x,0) = 7, \qquad p(x,0) = 0.2, \qquad u(x,0) = \begin{cases} -1, & -1 \le x < 0, \\ 1, & 0 < x \le 1. \end{cases}$$

The outflow boundary conditions are use at $x = -1$ and $x = 1$. A PP limiter is needed for this problem due to the appearance of extremely low density and pressure at the center of the domain. We simulate the problem up to $T = 0.6$. The numerical results at $T = 0.6$ of all the methods on a computational mesh with 500 cells are plotted in Fig. 7.2, together with a reference solution obtained with much refined 2000 cells. It can be seen that the structure of low-density and low-pressure waves can be well captured by all three methods.

Example 4. (Leblanc shock tube). We focus on an extension of the 1D Leblanc shock tube problem with the linear gravitational field $\phi(x) = x$. The initial solutions are given as follows

$$(\rho, u, p)(x,0) = \begin{cases} (2,\ 0,\ 10^9), & 0 \le x < 5, \\ (10^{-3},\ 0,\ 1), & 5 < x \le 10. \end{cases}$$

Reflection boundary conditions are arranged on both sides. The numerical results at $T = 0.00004$ of the proposed methods on 1600 cells are shown in Fig. 7.3, compared with a reference solution obtained on 6400 cells. We can observe that strong shocks are well captured by all the methods with high resolution.

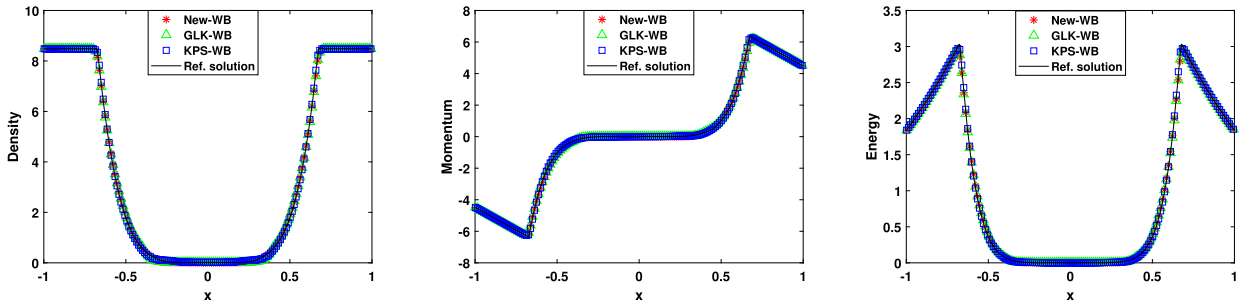

Fig. 7.2. Example 3, density, momentum and energy obtained by three methods with 500 cells. Left: ρ, Middle: m, Right: E.

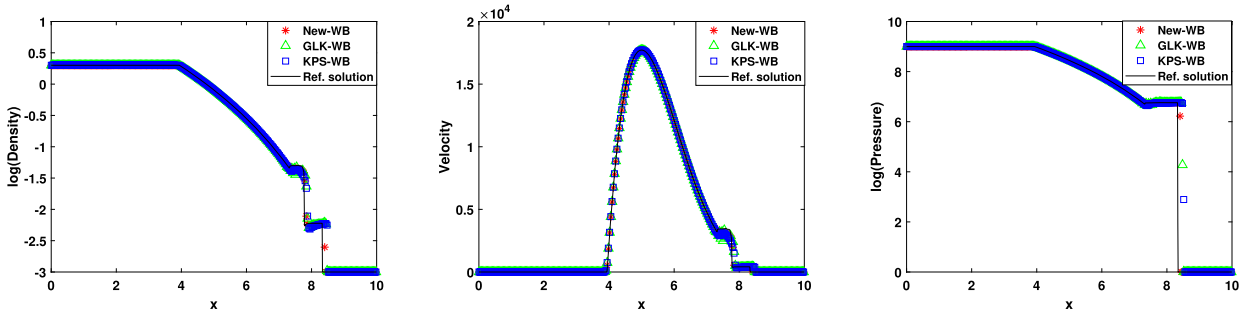

Fig. 7.3. Example 4: log plot of density, velocity, and log plot of pressure obtained by three methods with 1600 cells. Left: ρ, Middle: u, Right: p.

Example 5 (2D accuracy test). In this test case, we test the convergence rate of three methods in the 2D case. A linear gravitational potential function is given by $\phi_x = \phi_y = 1$ in the computational domain $\Omega = [0, 2]^2$. The exact solutions are given as follows

$$\begin{aligned} &\rho(x, y, t) = 1 + 0.2sin(\pi(x + y - t(u_0 + v_0))), \quad u(x, y) = v(x, y) = 1, \\ &p(x, y, t) = p_0 + t(u_0 + v_0) - x - y + \frac{0.2}{\pi} cos(\pi(x + y - t(u_0 + v_0))), \end{aligned} \tag{7.2}$$

with $u_0 = v_0 = 1$ and $p_0 = 4.5$ and the adiabatic index $\gamma = 5/3$. The boundary conditions are specified by the exact solutions on $\partial\Omega$. We compute the problem up to $T = 0.1$. The L_1 errors and the corresponding orders of convergence obtained by the proposed approaches on different meshes are listed in Table 7.4. We can observe that the expected high-order convergence rate is achieved for all three methods. In addition, the modified HLLC flux and the non-trivial source term approximation do not destroy the accuracy of the `New-WB` method.

Example 6 (2D polytropic equilibrium). The purpose of this example is to verify the well-balancedness of three methods in the polytropic case and their performance in capturing small perturbations of such solutions. We consider a static adiabatic gaseous sphere, which is held together by self-gravitation and can be constructed from the hydrostatic equilibrium $\frac{dp}{dr} = -\rho\frac{d\phi}{dr}$ with $\gamma = 2$. The equilibrium solutions take the form

$$\rho(r) = \rho_c \frac{sin(\alpha r)}{\alpha r}, \; u(r) = 0, \; v(r) = 0, \; p(r) = K_0\rho(r)^2, \tag{7.3}$$

under the gravitational field

$$\phi(r) = -2K_0\rho_c \frac{sin(\alpha r)}{\alpha r}, \tag{7.4}$$

where $\alpha = \sqrt{2\pi g/K_0}$ with $K_0 = g = \rho_c = 1$, and $r = \sqrt{x^2 + y^2}$ denotes the radial variable. The computational domain is taken as $[-0.5, 0.5]^2$. To validate the WB property, we use double precision to perform the computation with the initial data (7.3) up to $T = 1$ on different meshes. The L_1 errors are presented in Table 7.5. As expected, the steady-state solutions are maintained up to the round-off errors, which shows the well-balancedness of three methods. For a long time simulation, the errors of `New-WB` method will be slightly larger compared to the other two methods. This difference can be attributed to the use of different numerical fluxes. Specifically, the `New-WB` method utilizes the HLLC flux, while the other two schemes use the LF flux. Numerical investigation demonstrates that different numerical fluxes (LF and HLLC) for the same `KPS-WB` or

Table 7.4
Example 5. L_1 errors and convergence rates of three methods.

New-WB								
N	ρ		m		n		E	
8	3.34e-04	–	3.50e-04	–	3.50e-04	–	5.01e-04	–
16	1.18e-05	4.81	1.27e-05	4.77	1.27e-05	4.77	1.80e-05	4.79
32	3.83e-07	4.95	4.05e-07	4.97	4.05e-07	4.97	5.85e-07	4.94
64	1.19e-08	5.00	1.26e-08	5.00	1.26e-08	5.00	1.83e-08	4.99
GLK-WB								
N	ρ		m		n		E	
8	1.08e-03	–	1.09e-03	–	1.09e-03	–	1.25e-03	–
16	4.30e-05	4.65	4.32e-05	4.66	4.32e-05	4.66	4.72e-05	4.73
32	1.46e-06	4.88	1.46e-06	4.88	1.46e-06	4.88	1.59e-06	4.89
64	5.13e-08	4.83	5.12e-08	4.83	5.12e-08	4.83	5.58e-08	4.83
KPS-WB								
N	ρ		m		n		E	
8	1.08e-03	–	1.09e-03	–	1.09e-03	–	1.24e-03	–
16	4.25e-05	4.67	4.27e-05	4.67	4.27e-05	4.67	4.58e-05	4.76
32	1.40e-06	4.92	1.41e-06	4.92	1.41e-06	4.92	1.47e-06	4.95
64	4.43e-08	4.98	4.47e-08	4.97	4.47e-08	4.97	4.50e-08	5.03

Table 7.5
Example 6. L_1 errors of three methods with equilibrium initial data at $T = 1$.

New-WB				
N	ρ	m	n	E
20	5.94e-17	6.54e-16	6.98e-16	5.71e-16
40	5.93e-17	8.44e-16	8.51e-16	4.94e-16
GLK-WB				
N	ρ	m	n	E
20	1.63e-15	5.99e-16	6.03e-16	9.96e-16
40	2.76e-15	5.50e-16	5.68e-16	1.78e-15
KPS-WB				
N	ρ	m	n	E
20	5.75e-17	5.28e-16	5.75e-16	5.72e-17
40	5.83e-17	7.35e-16	7.54e-16	4.98e-17

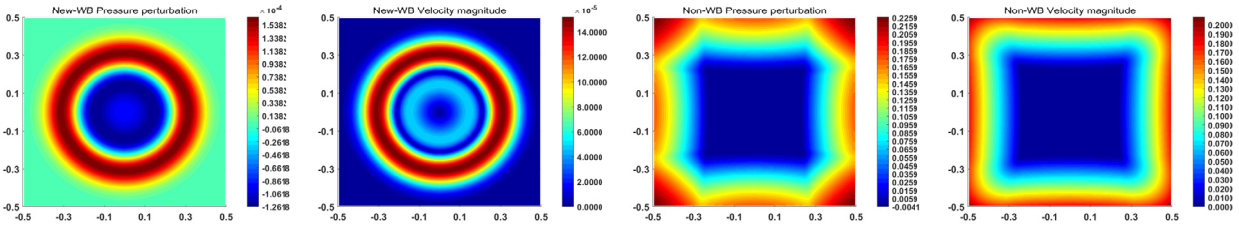

Fig. 7.4. Example 6: From left to right: New-WB pressure perturbation; New-WB velocity magnitude; non-WB pressure perturbation; non-WB velocity magnitude.

New-WB method yield comparable errors for cases with small stopping times and the scheme using the HLLC flux exhibited larger errors when the stopping time is large.

Next, we impose a small perturbation to the initial pressure state

$$p(r) = K_0 \rho(r)^2 + \eta \exp(-100r^2)$$

with $\eta = 10^{-3}$ and simulate the problem up to $T = 0.2$ using the New-WB method on 100×100 uniform cells. The transmissive boundary conditions are used. Fig. 7.4 shows the contour plots of the pressure perturbation and density velocity magnitude $r = \sqrt{u^2 + v^2}$. The non-WB method was not able to capture such a small perturbation well on coarse mesh, whereas the WB method performs very well.

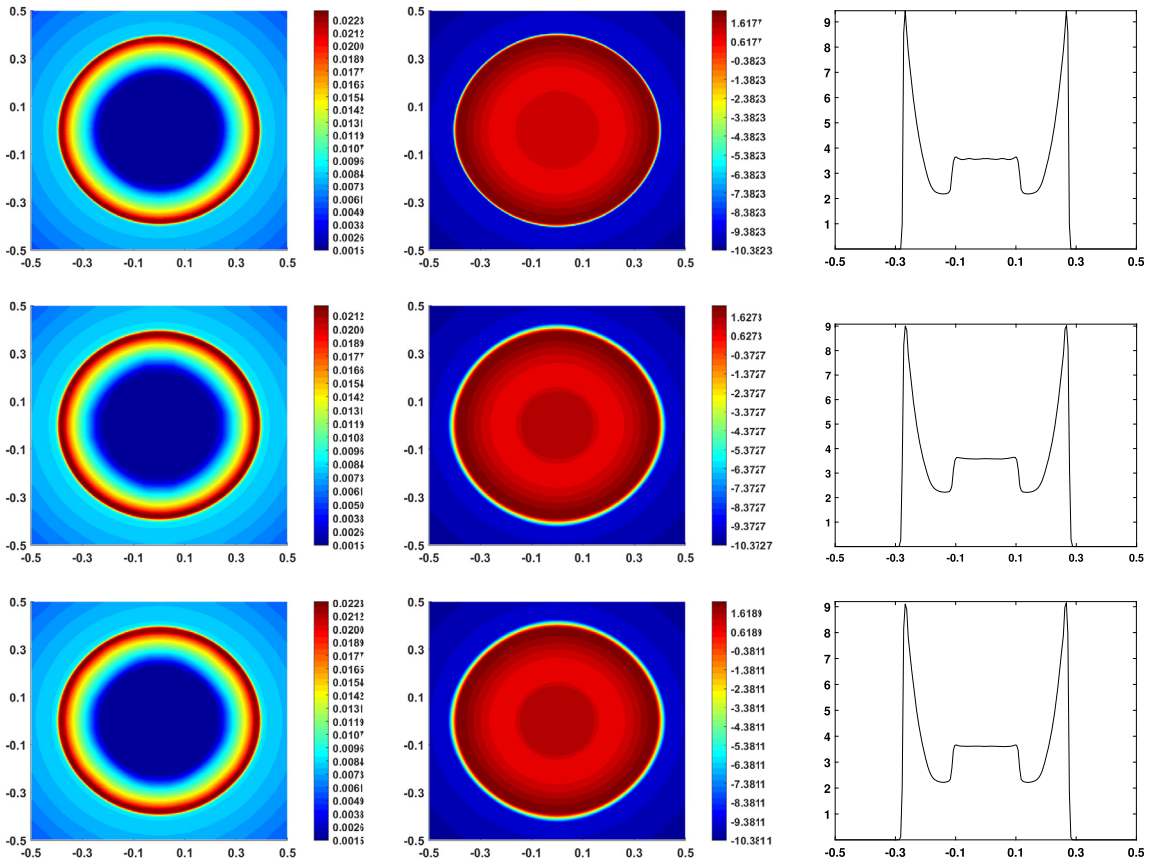

Fig. 7.5. Example 7: From top to bottom: `New-WB`; `GLK-WB`; `KPS-WB`; From left to right: ρ, $log(p)$, p along the line $y = x$.

Example 7 (2D blast problem). The purpose of this example is to verify the PP performance of three methods in the 2D case, where strong discontinuity also exists. We consider a 2D blast problem under the gravitational field (7.4). The initial data is obtained by adding a huge jump to the pressure term of the equilibrium (7.3), that is

$$p(x, y, 0) = K_0 \rho(r)^2 + \begin{cases} 100, & r < 0.1, \\ 0, & r > 0.1. \end{cases}$$

We set $K_0 = g = 1$ and $\gamma = 2$, and $\rho_c = 0.01$ which leads to the appearance of low pressure and low density in the solution. Again, the transmissive boundary conditions are considered. Fig. 7.5 shows surface plots of ρ and $log(p)$ at $T = 0.005$ computed by three methods with 200×200 cells. We also present the plot of p along the line $y = x$, and a strong shock can be observed at $\sqrt{x^2 + y^2}/\sqrt{2} \approx 0.28$. All three methods preserve the positivity of density and pressure and the axisymmetric structure of the solution well.

Example 8 (Inertia-gravity wave). This is a benchmark test problem arising from atmospheric flows and the setup follows [11,12]. The computational domain is a $[0, 300000] \times [0, 10000]$ m^2 channel, with inviscid wall boundary conditions on the bottom and top boundaries, and periodic boundary conditions on the left and right boundaries. The linear gravitational fields are taken as $\phi_x = 0$ and $\phi_y = g = 9.8$ m/s^2. A constant velocity is considered as $\mathbf{u} = (20\ \text{m/s}, 0\ \text{m/s})$, and the potential temperature and Exner pressure are given by

$$\Theta = T_0 \exp\left(\frac{\mathcal{N}^2}{g} y\right), \qquad \Pi = 1 + \frac{(\gamma - 1) g^2}{\gamma R T_0 \mathcal{N}^2} \left[\exp\left(-\frac{\mathcal{N}^2}{g} y\right) - 1\right],$$

where the Brunt–Väisälä frequency $\mathcal{N} = 0.01$ /s, the reference temperature $T_0 = 300$ K at $y = 0$ m, and the gas constant $R = 287.058$ J/kg K. Initially, a small perturbation is added to the potential temperature: $\Delta\Theta(x, y, 0) = \theta_c \sin\left(\frac{\pi y}{h_c}\right) \left[1 + (x - x_c)^2 / a_c^2\right]^{-1}$, where $\theta_c = 0.01$ K, $h_c = 10000$ m, $x_c = 100000$ m, and $a_c = 5000$ m. The pressure and density are computed by Θ and Π via

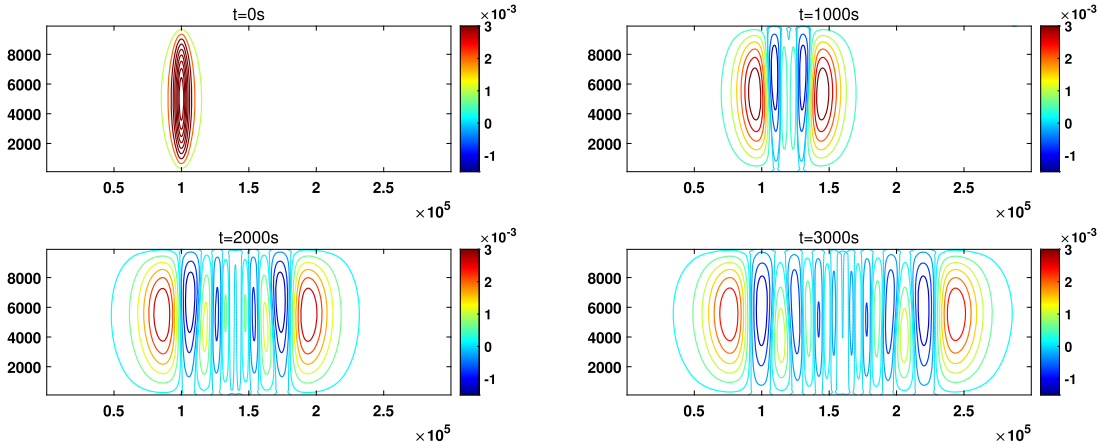

Fig. 7.6. Example 8: Top-Left: $\Delta\Theta(x, y, t = 0\ \text{s})$; Top-Right: $\Delta\Theta(x, y, t = 1000\ \text{s})$; Bottom-Left: $\Delta\Theta(x, y, t = 2000\ \text{s})$; Bottom-Right: $\Delta\Theta(x, y, t = 3000\ \text{s})$.

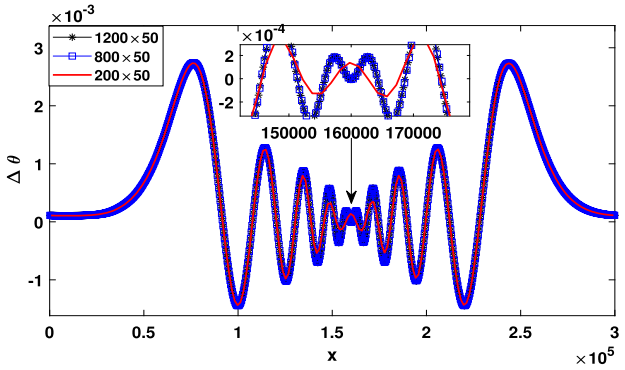

Fig. 7.7. Example 8 with `New-WB`: $\Delta\Theta(x, y, t = 3000\ \text{s})$ along with $y = 5000$m.

$$p = p_0 \Pi^{\frac{\gamma}{\gamma-1}}, \qquad \rho = \frac{p_0}{R\Theta} \Pi^{\frac{1}{\gamma-1}}, \tag{7.5}$$

with the reference pressure $p_0 = 10^5$ N/m^2 at $y = 0$ m.

We compute this problem up to $T = 3000$ s on a mesh of 1200×50 uniform cells using the proposed `New-WB` method. The contours of the potential temperature perturbation at various times, $\Delta\Theta(x, y, t = 0\ \text{s})$, $\Delta\Theta(x, y, t = 1000\ \text{s})$, $\Delta\Theta(x, y, t = 2000\ \text{s})$ and $\Delta\Theta(x, y, t = 3000\ \text{s})$, are presented in Fig. 7.6. In addition, Fig. 7.7 displays the profiles of $\Delta\Theta(x, y = 5000\ \text{m}, t = 3000\ \text{s})$ on different mesh sizes. We observe that the evolution of potential temperature perturbation can be well captured and that the solution structures agree well with those presented in [11,12].

Remark 7.1. In the numerical implementation of Example 8, we adopted the following boundary treatment method. Let S and S^e represent numerical solutions and equilibrium solutions. Denote the perturbation by $\mathrm{P} = \mathrm{S} - \mathrm{S}^e$. The inviscid boundary and periodic boundary conditions are applied to the variable P only, and the values of S in the ghost cells can be obtained by $\mathrm{S} = \mathrm{P} + \mathrm{S}^e$, where the values of S^e in the ghost cells are known. Note that this boundary treatment does not affect the WB property of the scheme.

Example 9 (Rising thermal bubble). The last example is also a benchmark test problem for atmospheric flows, and simulates the dynamics of a warm bubble. The setup follows that in [11,12]. The computational domain is $[0, 1000] \times [0, 1000]\text{m}^2$ and the inviscid wall boundary conditions are applied, with the boundary treatment in Remark 7.1. A linear gravitational field is given by $\phi_x = 0$ and $\phi_y = g = 9.8$ m/s^2. Here we consider a stratified atmosphere, with zero velocity $\mathbf{u} = \mathbf{0}$, a constant potential temperature $\Theta = T_0 = 300$ K, and Exner pressure $\Pi = 1 - \frac{(\gamma-1)gy}{\gamma R T_0}$, where $R = 287.058$ J/kg K is the gas constant. Initially, the warm bubble is added as a potential temperature perturbation to the hydrostatic balance

$$\Delta\Theta(x, y, t = 0) = \begin{cases} 0, & r > r_c \\ \frac{\theta_c}{2}\left(1 + \cos(\pi r / r_c)\right), & r \le r_c, \end{cases} \qquad r = \sqrt{(x - x_c)^2 + (y - y_c)^2},$$

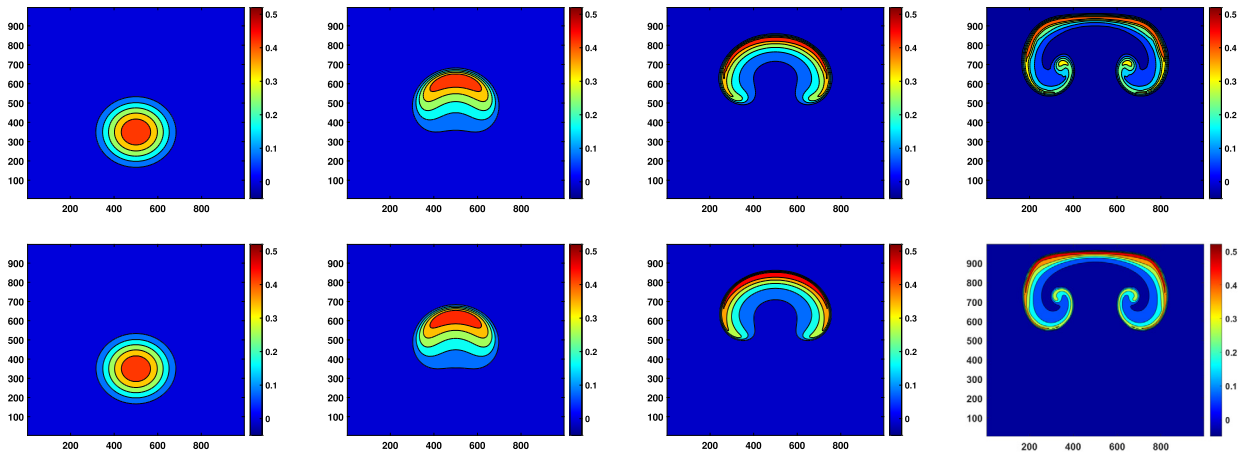

Fig. 7.8. Example 9: The potential temperature perturbation $\Delta\Theta$. From left to right: $t = 0$s, $t = 300$s, $t = 500$s, $t = 700$s; Top: 100×100 cells; Bottom: 200×200 cells.

where $\theta_c = 0.5$ K, $(x_c, y_c) = (500, 350)$ m, and $r_c = 250$ m. The pressure and density are computed by Θ and Π via the formulas in (7.5), with the reference pressure $p_0 = 10^5$ N/m^2. Fig. 7.8 demonstrates the potential temperature perturbation $\Delta\Theta$ obtained by the `New-WB` method on 100×100 cells (10m resolution) and 200×200 cells (5m resolution), respectively. It can be observed that the initial circular bubble deforms into a mushroom-shaped cloud, and this solution is very consistent with the solution proposed in [11,12].

8. Conclusions

This paper presented three high-order structure-preserving FV WENO methods for the Euler equations with gravitation, based on a newly developed scheme and two schemes proposed in [15,20]. A notable feature of these three methods is that they are not only WB for hydrostatic equilibrium states but also preserve the positivity of density and pressure. They were built on a simple local scaling PP limiter and a modified WENO-ZQ reconstruction exactly preserving the cell average value and scaling invariance. We introduced suitable numerical fluxes and approximations to the gravitational source terms for the three methods to achieve the WB property. Based on some convex decomposition techniques as well as several critical properties of the admissible states and numerical flux, we carried out rigorous positivity-preserving analyses for these three WB schemes. We rigorously proved that the three WB methods, coupled with the PP limiter and a strong-stability-preserving time discretization, are always PP under suitable CFL conditions. Extensive numerical examples were provided to confirm the WB and PP properties of the three methods.

At the end, we would like to provide an quick overview of the three methods in terms of relative accuracy, computational cost, and time step restrictions. Numerical tests have demonstrated that the errors of the three methods are comparable under the same fifth-order accuracy, especially in simulations with small termination times. In terms of CPU time, the numerical examples indicate that the `New-WB` method and the `KPS-WB` method have comparable computation times, which is less than that of the `GLK-WB` method. Regarding the CFL condition, all three methods have the same CFL condition when considering only the WB property. However, when taking the theoretical PP property into account, the CFL condition is influenced by the value of ω_1. For fifth-order schemes, both the `New-WB` and `GLK-WB` methods have $\omega_1 = 1/12$, while the `KPS-WB` method has $\omega_1 = 7/90$ which is slightly smaller.

CRediT authorship contribution statement

Yupeng Ren: Conceptualization, Methodology, Software, Validation, Visualization, Writing – original draft. **Kailiang Wu:** Conceptualization, Methodology, Supervision, Writing – original draft. **Jianxian Qiu:** Conceptualization, Methodology, Supervision, Writing – original draft. **Yulong Xing:** Conceptualization, Methodology, Supervision, Validation, Writing – original draft.

Declaration of competing interest

The authors declare the following financial interests/personal relationships which may be considered as potential competing interests:

Yulong Xing reports financial support was provided by National Science Foundation. Kailiang Wu reports financial support was provided by National Natural Science Foundation of China. Jianxian Qiu reports financial support was provided by National Natural Science Foundation of China. Jianxian Qiu reports financial support was provided by National Key Research

and Development Program of China. Co-author serves as an editorial board member of Journal of Computational Physics – Jianxian Qiu.

Data availability

Data will be made available on request.

Appendix A. A_j in the KPS-WB method

1D case: We are taking the sixth order source term discretization ($l=2$ in (6.7)) as an example to illustrate it. We decompose cell $I_j=[x_{j-\frac{1}{2}},x_{j+\frac{1}{2}}]$ into $2^l=4$ subcells as shown in Fig. A.9, where x_j^κ are quadrature nodes, $I_{j_\kappa}=x_j^{\kappa+1}-x_j^\kappa$ with $\kappa=1,\cdots,4$, and $I_{j_{12}}=I_{j_1}\cup I_{j_2}$ and $I_{j_{34}}=I_{j_3}\cup I_{j_4}$.

We define $(\overline{f(x)})_{j,j_n}$ as the average value of $f(x)$ on the subcell I_{j_n} of the cell I_j. For example, $(\overline{f})_{j,j_1}=\frac{4}{\Delta x}\int_{I_{j_1}}f\,dx$ and $(\overline{f})_{j,j_{12}}=\frac{2}{\Delta x}\int_{I_{j_{12}}}f\,dx$. To simplify the notation, we use the ρ_κ instead of $\rho(x_j^\kappa)$, and ρ_κ^e and p_κ^e defined similarly. Hence, for the discretization of the source term in the momentum equation, we have (after applying Romberg's method twice)

$$\begin{aligned}
\overline{S}_j^{[2]} &= \frac{32}{45}\left((\frac{\rho_1}{\rho_1^e}+\frac{\rho_2}{\rho_2^e})\frac{p_2^e-p_1^e}{\Delta x}+(\frac{\rho_2}{\rho_2^e}+\frac{\rho_3}{\rho_3^e})\frac{p_3^e-p_2^e}{\Delta x}+(\frac{\rho_3}{\rho_3^e}+\frac{\rho_4}{\rho_4^e})\frac{p_4^e-p_3^e}{\Delta x}+(\frac{\rho_4}{\rho_4^e}+\frac{\rho_5}{\rho_5^e})\frac{p_5^e-p_4^e}{\Delta x}\right)\\
&-\frac{10}{45}\left((\frac{\rho_1}{\rho_1^e}+\frac{\rho_3}{\rho_3^e})\frac{p_3^e-p_1^e}{\Delta x}+(\frac{\rho_3}{\rho_3^e}+\frac{\rho_5}{\rho_5^e})\frac{p_5^e-p_3^e}{\Delta x}\right)+\frac{1}{90}(\frac{\rho_1}{\rho_1^e}+\frac{\rho_5}{\rho_5^e})\frac{p_5^e-p_1^e}{\Delta x}\\
&=\frac{7}{90}\frac{\rho_1}{\rho_1^e}\left(\frac{1}{7}\left(16(\overline{p_x^e})_{j,j_1}-10(\overline{p_x^e})_{j,j_{12}}+(\overline{p_x^e})_j\right)\right)+\frac{16}{45}\frac{\rho_2}{\rho_2^e}\left(\frac{1}{2}\left((\overline{p_x^e})_{j,j_1}+(\overline{p_x^e})_{j,j_2}\right)\right)\\
&+\frac{6}{45}\frac{\rho_3}{\rho_3^e}\left(\frac{1}{6}\left(8(\overline{p_x^e})_{j,j_2}+8(\overline{p_x^e})_{j,j_3}-5(\overline{p_x^e})_{j,j_{12}}-5(\overline{p_x^e})_{j,j_{34}}\right)\right)\\
&+\frac{16}{45}\frac{\rho_4}{\rho_4^e}\left(\frac{1}{2}\left((\overline{p_x^e})_{j,j_3}+(\overline{p_x^e})_{j,j_4}\right)\right)+\frac{7}{90}\frac{\rho_5}{\rho_5^e}\left(\frac{1}{7}\left(16(\overline{p_x^e})_{j,j_4}-10(\overline{p_x^e})_{j,j_{34}}+(\overline{p_x^e})_j\right)\right)\\
&=\sum_{\kappa=1}^{5}\omega_\kappa\frac{\rho_\kappa}{\rho_\kappa^e}A_j^\kappa,
\end{aligned}$$

where $\omega=[\frac{7}{90},\frac{16}{45},\frac{6}{45},\frac{16}{45},\frac{7}{90}]$ is the Romberg's quadrature weights, and

$$A_j=\begin{pmatrix}
\frac{1}{7}\left(16(\overline{p_x^e})_{j,j_1}-10(\overline{p_x^e})_{j,j_{12}}+(\overline{p_x^e})_j\right)\\
\frac{1}{2}\left((\overline{p_x^e})_{j,j1}+(\overline{p_x^e})_{j,j_2}\right)\\
\frac{1}{6}\left(8(\overline{p_x^e})_{j,j_2}+8(\overline{p_x^e})_{j,j_3}-5(\overline{p_x^e})_{j,j_{12}}-5(\overline{p_x^e})_{j,j_{34}}\right)\\
\frac{1}{2}\left((\overline{p_x^e})_{j,j_3}+(\overline{p_x^e})_{j,j_4}\right)\\
\frac{1}{7}\left(16(\overline{p_x^e})_{j,j_4}-10(\overline{p_x^e})_{j,j_{34}}+(\overline{p_x^e})_j\right)
\end{pmatrix}. \tag{A.6}$$

The definition of $\overline{S}_j^{[3]}$ is similar to $\overline{S}_j^{[2]}$ for this sixth order scheme, with the only difference being $\rho_\kappa/\rho_\kappa^e$ replaced by m_κ/ρ_κ^e.

Similarly, for the fourth-order source term approximation, the form of A_j can be obtained as

$$\begin{aligned}
\overline{S}_j^{[2]} &= \frac{4}{3}\left(\frac{1}{2}(\frac{\rho_1}{\rho_1^e}+\frac{\rho_3}{\rho_3^e})\frac{p_3^e-p_1^e}{\Delta x}+\frac{1}{2}(\frac{\rho_3}{\rho_3^e}+\frac{\rho_5}{\rho_5^e})\frac{p_5^e-p_3^e}{\Delta x}\right)-\frac{1}{3}\left(\frac{1}{2}(\frac{\rho_1}{\rho_1^e}+\frac{\rho_5}{\rho_5^e})\frac{p_5^e-p_1^e}{\Delta x}\right)\\
&=\frac{1}{6}\frac{\rho_1}{\rho_1^e}\left(2(\overline{p_x^e})_{j,j_{12}}-(\overline{p_x^e})_j\right)+\frac{4}{6}\frac{\rho_3}{\rho_3^e}\left(\frac{1}{2}(\overline{p_x^e})_{j,j_{12}}+\frac{1}{2}(\overline{p_x^e})_{j,j_{34}}\right)+\frac{1}{6}\frac{\rho_5}{\rho_5^e}\left(2(\overline{p_x^e})_{j,j_{34}}-(\overline{p_x^e})_j\right)
\end{aligned}$$

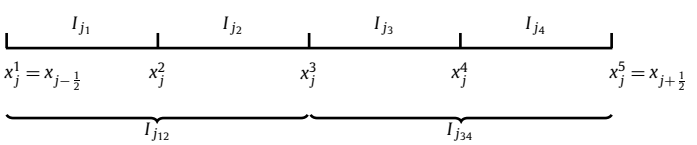

Fig. A.9. Segment for sixth order Romberg's method.

$$= \sum_{\kappa=1}^{3} \omega_\kappa \frac{\rho_\kappa}{\rho_\kappa^e} A_j^\kappa,$$

where $\omega = [\frac{1}{6}, \frac{4}{6}, \frac{1}{6}]$ and $A_j = \left(2(\overline{p_x^e})_{j,j_{12}} - (\overline{p_x^e})_j, \frac{1}{2}(\overline{p_x^e})_{j,j_{12}} + \frac{1}{2}(\overline{p_x^e})_{j,j_{34}}, 2(\overline{p_x^e})_{j,j_{34}} - (\overline{p_x^e})_j\right)^\top$. Finally, for the second-order scheme, we have $\omega = (\frac{1}{2}, \frac{1}{2})$ and $A_j = ((\overline{p_x^e})_j, (\overline{p_x^e})_j)^\top$.

2D case: Following a similar way as in the 1D case, we can express τ^x and τ^y for $l = 2$ as follows:

$$(\tau^x)_{5\times 5} = \left(\tau_1^x, \cdots, \tau_5^x\right), \qquad (\tau^y)_{5\times 5} = \begin{pmatrix} \tau_1^y \\ \vdots \\ \tau_5^y \end{pmatrix}, \tag{A.7}$$

where

$$\tau_\kappa^x := \begin{pmatrix} \frac{1}{7}\left(16(\overline{p_x^e(x, y_j^\kappa)})_{I_{ij},i_1} - 10(\overline{p_x^e(x, y_j^\kappa)})_{I_{ij},i_{12}} + (\overline{p_x^e(x, y_j^\kappa)})_i\right) \\ \frac{1}{2}\left((\overline{p_x^e(x, y_j^\kappa)})_{I_{ij},i_1} + (\overline{p_x^e(x, y_j^\kappa)})_{I_{ij},i_2}\right) \\ \frac{1}{6}\left(8(\overline{p_x^e(x, y_j^\kappa)})_{I_{ij},i_2} + 8(\overline{p_x^e(x, y_j^\kappa)})_{I_{ij},i_3} - 5(\overline{p_x^e(x, y_j^\kappa)})_{I_{ij},i_{12}} - 5(\overline{p_x^e(x, y_j^\kappa)})_{I_{ij},i_{34}}\right) \\ \frac{1}{2}\left((\overline{p_x^e(x, y_j^\kappa)})_{I_{ij},i_3} + (\overline{p_x^e(x, y_j^\kappa)})_{I_{ij},i_4}\right) \\ \frac{1}{7}\left(16(\overline{p_x^e(x, y_j^\kappa)})_{I_{ij},i_4} - 10(\overline{p_x^e(x, y_j^\kappa)})_{I_{ij},i_{34}} + (\overline{p_x^e(x, y_j^\kappa)})_i\right) \end{pmatrix}, \tag{A.8}$$

$$\tau_\kappa^y := \begin{pmatrix} \frac{1}{7}\left(16(\overline{p_y^e(x_i^\kappa, y)})_{I_{ij},j_1} - 10(\overline{p_y^e(x_i^\kappa, y)})_{I_{ij},j_{12}} + (\overline{p_y^e(x_i^\kappa, y)})_j\right) \\ \frac{1}{2}\left((\overline{p_y^e(x_i^\kappa, y)})_{I_{ij},j_1} + (\overline{p_y^e(x_i^\kappa, y)})_{I_{ij},j_2}\right) \\ \frac{1}{6}\left(8(\overline{p_y^e(x_i^\kappa, y)})_{I_{ij},j_2} + 8(\overline{p_y^e(x_i^\kappa, y)})_{I_{ij},j_3} - 5(\overline{p_y^e(x_i^\kappa, y)})_{I_{ij},j_{12}} - 5(\overline{p_y^e(x_i^\kappa, y)})_{I_{ij},j_{34}}\right) \\ \frac{1}{2}\left((\overline{p_y^e(x_i^\kappa, y)})_{I_{ij},j_3} + (\overline{p_y^e(x_i^\kappa, y)})_{I_{ij},j_4}\right) \\ \frac{1}{7}\left(16(\overline{p_y^e(x_i^\kappa, y)})_{I_{ij},j_4} - 10(\overline{p_y^e(x_i^\kappa, y)})_{I_{ij},j_{34}} + (\overline{p_y^e(x_i^\kappa, y)})_{I_{ij},j}\right) \end{pmatrix}^\top, \tag{A.9}$$

for $\kappa = 1, \cdots, 5$. The values of τ^x and τ^y for the fourth- and second-order source term approximations follow a similar analysis and are skipped here.

References

[1] E. Audusse, F. Bouchut, M.-O. Bristeau, R. Klein, B. Perthame, A fast and stable well-balanced scheme with hydrostatic reconstruction for shallow water flows, SIAM J. Sci. Comput. 25 (2004) 2050–2065.
[2] P. Batten, N. Clarke, C. Lambert, D.M. Causon, On the choice of wavespeeds for the HLLC Riemann solver, SIAM J. Sci. Comput. 18 (1997) 1553–1570.
[3] J.P. Berberich, R. Käppeli, P. Chandrashekar, C. Klingenberg, High-order discretely well-balanced methods for arbitrary hydrostatic atmospheres, Commun. Comput. Phys. 30 (2021) 666–708.
[4] N. Botta, R. Klein, S. Langenberg, S. Lützenkirchen, Well-balanced finite volume methods for nearly hydrostatic flows, J. Comput. Phys. 196 (2004) 539–565.
[5] X. Cai, X. Zhang, J. Qiu, Positivity-preserving high order finite volume HWENO schemes for compressible Euler equations, J. Sci. Comput. 68 (2016) 464–483.
[6] P. Chandrashekar, C. Klingenberg, A second order well-balanced finite volume scheme for Euler equations with gravity, SIAM J. Sci. Comput. 37 (2015) B382–B402.
[7] P. Chandrashekar, M. Zenk, Well-balanced nodal discontinuous Galerkin method for Euler equations with gravity, J. Sci. Comput. 71 (2017) 1062–1093.
[8] Y. Chen, K. Wu, A physical-constraint-preserving finite volume WENO method for special relativistic hydrodynamics on unstructured meshes, J. Comput. Phys. 466 (2022) 111398.
[9] A. Chertock, S. Cui, A. Kurganov, Ş.N. Özcan, E. Tadmor, Well-balanced schemes for the Euler equations with gravitation: conservative formulation using global fluxes, J. Comput. Phys. 358 (2018) 36–52.
[10] E. Franck, L.S. Mendoza, Finite volume scheme with local high order discretization of the hydrostatic equilibrium for the Euler equations with external forces, J. Sci. Comput. 69 (2016) 314–354.
[11] D. Ghosh, E.M. Constantinescu, Well-balanced, conservative finite difference algorithm for atmospheric flows, AIAA J. 54 (2016) 1370–1385.
[12] F.X. Giraldo, M. Restelli, A study of spectral element and discontinuous Galerkin methods for the Navier–Stokes equations in nonhydrostatic mesoscale atmospheric modeling: equation sets and test cases, J. Comput. Phys. 227 (2008) 3849–3877.
[13] S. Gottlieb, C.-W. Shu, E. Tadmor, Strong stability-preserving high-order time discretization methods, SIAM Rev. 43 (2001) 89–112.
[14] J.M. Greenberg, A.Y. LeRoux, A well-balanced scheme for the numerical processing of source terms in hyperbolic equations, SIAM J. Numer. Anal. 33 (1996) 1–16.
[15] L. Grosheintz-Laval, R. Käppeli, High-order well-balanced finite volume schemes for the Euler equations with gravitation, J. Comput. Phys. 378 (2019) 324–343.
[16] X.Y. Hu, N.A. Adams, C.-W. Shu, Positivity-preserving method for high-order conservative schemes solving compressible Euler equations, J. Comput. Phys. 242 (2013) 169–180.
[17] H. Jiang, H. Tang, K. Wu, Positivity-preserving well-balanced central discontinuous Galekin schemes for the Euler equations under gravitational fields, J. Comput. Phys. 463 (2022) 111297.

[18] R. Käppeli, S. Mishra, Well-balanced schemes for the Euler equations with gravitation, J. Comput. Phys. 259 (2014) 199–219.
[19] R. Käppeli, S. Mishra, A well-balanced finite volume scheme for the Euler equations with gravitation — the exact preservation of hydrostatic equilibrium with arbitrary entropy stratification, Astron. Astrophys. 587 (2016) A94.
[20] C. Klingenberg, G. Puppo, M. Semplice, Arbitrary order finite volume well-balanced schemes for the Euler equations with gravity, SIAM J. Sci. Comput. 41 (2019) A695–A721.
[21] A. Kurganov, G. Petrova, et al., A second-order well-balanced positivity preserving central-upwind scheme for the Saint–Venant system, Commun. Math. Sci. 5 (2007) 133–160.
[22] R.J. LeVeque, D.S. Bale, Wave propagation methods for conservation laws with source terms, in: Proceedings of the 7th International Conference on Hyperbolic Problems, 1998, pp. 609–618.
[23] G. Li, Y. Xing, High-order finite volume WENO schemes for the Euler equations under gravitational fields, J. Comput. Phys. 316 (2016) 145–163.
[24] G. Li, Y. Xing, Well-balanced discontinuous Galerkin methods for the Euler equations under gravitational fields, J. Sci. Comput. 67 (2016) 493–513.
[25] G. Li, Y. Xing, Well-balanced discontinuous Galerkin methods with hydrostatic reconstruction for the Euler equations with gravitation, J. Comput. Phys. 352 (2018) 445–462.
[26] G. Li, Y. Xing, Well-balanced finite difference weighted essentially non-oscillatory schemes for the Euler equations with static gravitational fields, Comput. Math. Appl. 75 (2018) 2071–2085.
[27] J. Luo, K. Xu, N. Liu, A well-balanced symplecticity-preserving gas-kinetic scheme for hydrodynamic equations under gravitational field, SIAM J. Sci. Comput. 33 (2011) 2356–2381.
[28] C.-W. Shu, Bound-preserving high-order schemes for hyperbolic equations: survey and recent developments, in: C. Klingenberg, M. Westdickenberg (Eds.), Theory, Numerics and Applications of Hyperbolic Problems II, Springer International Publishing, Cham, 2018, pp. 591–603.
[29] E.F. Toro, Riemann Solvers and Numerical Methods for Fluid Dynamics: a Practical Introduction, Springer Science & Business Media, 2013.
[30] D. Varma, P. Chandrashekar, A second-order, discretely well-balanced finite volume scheme for Euler equations with gravity, Comput. Fluids 181 (2019) 292–313.
[31] M. Veiga, D.A. Velasco-Romero, R. Abgrall, R. Teyssier, Capturing near-equilibrium solutions: a comparison between high-order discontinuous Galerkin methods and well-balanced schemes, Commun. Comput. Phys. 26 (2019) 1–34.
[32] K. Wu, Design of provably physical-constraint-preserving methods for general relativistic hydrodynamics, Phys. Rev. D 95 (2017) 103001.
[33] K. Wu, Positivity-preserving analysis of numerical schemes for ideal magnetohydrodynamics, SIAM J. Numer. Anal. 56 (2018) 2124–2147.
[34] K. Wu, Minimum principle on specific entropy and high-order accurate invariant region preserving numerical methods for relativistic hydrodynamics, SIAM J. Sci. Comput. 43 (2021) B1164–B1197.
[35] K. Wu, C.-W. Shu, Provably positive high-order schemes for ideal magnetohydrodynamics: analysis on general meshes, Numer. Math. 142 (2019) 995–1047.
[36] K. Wu, C.-W. Shu, Geometric quasilinearization framework for analysis and design of bound-preserving schemes, SIAM Rev. (2022), in press.
[37] K. Wu, Y. Xing, Uniformly high-order structure-preserving discontinuous Galerkin methods for Euler equations with gravitation: positivity and well-balancedness, SIAM J. Sci. Comput. 43 (2021) A472–A510.
[38] K. Wu, H. Tang, High-order accurate physical-constraints-preserving finite difference WENO schemes for special relativistic hydrodynamics, J. Comput. Phys. 298 (2015) 539–564.
[39] Y. Xing, C.-W. Shu, High-order finite difference WENO schemes with the exact conservation property for the shallow water equations, J. Comput. Phys. 208 (2005) 206–227.
[40] Y. Xing, C.-W. Shu, High-order finite volume WENO schemes for the shallow water equations with dry states, Adv. Water Resour. 34 (2011) 1026–1038.
[41] Y. Xing, C.-W. Shu, High-order well-balanced WENO scheme for the gas dynamics equations under gravitational fields, J. Sci. Comput. 54 (2013) 645–662.
[42] Y. Xing, X. Zhang, Positivity-preserving well-balanced discontinuous Galerkin methods for the shallow water equations on unstructured triangular meshes, J. Sci. Comput. 57 (2013) 19–41.
[43] Y. Xing, X. Zhang, C.-W. Shu, Positivity-preserving high-order well-balanced discontinuous Galerkin methods for the shallow water equations, Adv. Water Resour. 33 (2010) 1476–1493.
[44] K. Xu, A well-balanced gas-kinetic scheme for the shallow-water equations with source terms, J. Comput. Phys. 178 (2002) 533–562.
[45] K. Xu, J. Luo, S. Chen, A well-balanced kinetic scheme for gas dynamic equations under gravitational field, Adv. Appl. Math. Mech. 2 (2010) 200–210.
[46] Z. Xu, Parametrized maximum principle preserving flux limiters for high-order schemes solving hyperbolic conservation laws: one-dimensional scalar problem, Math. Comput. 83 (2014) 2213–2238.
[47] X. Zhang, On positivity-preserving high-order discontinuous Galerkin schemes for compressible Navier-Stokes equations, J. Comput. Phys. 328 (2017) 301–343.
[48] X. Zhang, C.-W. Shu, Maximum-principle-satisfying and positivity-preserving high order schemes for conservation laws: survey and new developments, Proc. R. Soc. A 467 (2011) 2752–2776.
[49] X. Zhang, C.-W. Shu, On maximum-principle-satisfying high-order schemes for scalar conservation laws, J. Comput. Phys. 229 (2010) 3091–3120.
[50] X. Zhang, C.-W. Shu, On positivity-preserving high-order discontinuous Galerkin schemes for compressible Euler equations on rectangular meshes, J. Comput. Phys. 229 (2010) 8918–8934.
[51] X. Zhang, C.-W. Shu, Positivity-preserving high-order discontinuous Galerkin schemes for compressible Euler equations with source terms, J. Comput. Phys. 230 (2011) 1238–1248.
[52] W. Zhang, Y. Xing, Y. Xia, Y. Xu, High-order positivity-preserving well-balanced discontinuous Galerkin methods for Euler equations with gravitation on unstructured meshes, Commun. Comput. Phys. 31 (2022) 771–815.
[53] J. Zhu, J. Qiu, A new type of finite volume WENO schemes for hyperbolic conservation laws, J. Sci. Comput. 73 (2017) 1338–1359.